JACS
JOURNAL OF THE AMERICAN CHEMICAL SOCIETY
pubs.acs.org/JACS



Article

# The Role of Surface Complexes in Ketene Formation from Fatty Acids via Pyrolysis over Silica: from Platform Molecules to Waste Biomass

Liana R. Azizova,* Tetiana V. Kulik,* Borys B. Palianytsia, Mykola M. Ilchenko, German M. Telbiz, Alina M. Balu, Sergiy Tarnavskiy, Rafael Luque, Alberto Roldan, and Mykola T. Kartel

Cite This: https://doi.org/10.1021/jacs.3c06966

Read Online

ACCESS | Metrics & More | Article Recommendations | Supporting Information

**ABSTRACT:** Fatty acids (FA) are the main constituents of lipids and oil crop waste, considered to be a promising 2G biomass that can be converted into ketenes via catalytic pyrolysis. Ketenes are appraised as promising synthons for the pharmaceutical, polymer, and chemical industries. Progress in the thermal conversion of short- and long-chain fatty acids into ketenes requires a deep understanding of their interaction mechanisms with the nanoscale oxide catalysts. In this work, the interactions of fatty acids with silica are investigated using a wide range of experimental and computational techniques (TPD MS, DFT, FTIR, *in situ* IR, equilibrium adsorption, and thermogravimetry). The adsorption isotherms of linear and branched fatty acids C1−C6 on the silica surface from aqueous solution have been obtained. The relative quantities of different types of surface complexes, as well as kinetic parameters of their decomposition, were calculated. The formation of surface complexes with a coordination bond between the carbonyl oxygens and silicon atoms in the surface-active center, which becomes pentacoordinate, was confirmed by DFT calculations, in good agreement with the IR feature at ∼1680 cm $^{1}$. Interestingly, ketenes release relate to these complexes' decomposition as confirmed by the thermal evolution of the absorption band (1680 $cm^{-1}$) synchronously with the TPD peak of the ketene molecular ion. The established regularities of the ketenezation are also observed for the silica-induced pyrolysis of glyceryl trimyristate and real waste, rapeseed meals.

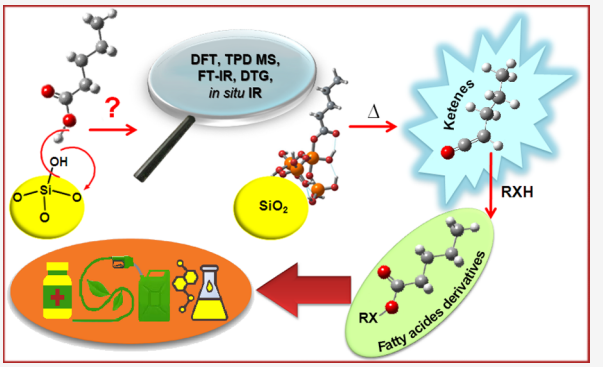




## 1. INTRODUCTION

Interest in the industrial application of vegetable oils and fats for developing renewable energy sources, biofuels, and oleochemicals has rapidly increased in recent years.[1] The hydrolysis of triglycerides into glycerine and mixed fatty acids is a major process to convert biomass into biobased chemicals and fuels.[2] Pyrolysis and thermochemical conversion of vegetable oils and fats into oleochemicals and fuels is inexpensive and requires mild temperatures.[3,4]

Fatty acids (FA) are main constituents of vegetable oils and fats.[2,5] Short-chain acids (ethanoic, butanoic, pentanoic, 4-oxopentanoic acid (levulinic), etc.) and various furan derivatives with a carboxyl group (furandicarboxylic acid, etc.) can be obtained in large volumes through biochemical and chemical catalysis of lignocellulosic biomass.[6,7] The short- and long-chain fatty acids and some other acids are used as platform molecules in biomass conversion technologies and as building blocks in producing pharmaceuticals, polymers, and fine chemicals.[8,9]

The catalytic pyrolysis of carboxylic acids is an environmentally benign, one-step process that avoids toxic reagents and solvents and does not generate harmful byproducts.[6,10] The most common catalysts are inorganic oxides based on Al, Si, Ti, Zr, Ce, Zn, Mg, Fe, Ni, Co, etc.[11,12] These catalysts are employed to obtain alkanes, aldehydes, ketones, and ketenes.[12−15] Among these inorganic supports, silica and its derivatives with controlled particle size, morphology, and surface area provide good mechanical properties, thermal stability, accessible functionalization properties, and resistance against attacks by organic solvents, making them popular catalysts for pyrolysis.[16]

Ketenes are widely used in industrial chemistry.[17] The catalytic production of ketenes by pyrolysis of carboxylic acids proceeds at lower temperatures and is less harmful to the environment than traditional synthesis methods.[18,19] The traditional methods of ketene production, such as thermal

Received: July 1, 2023
Revised: November 2, 2023
Accepted: November 6, 2023

pyrolysis of carboxylic acids and ketones, dehalogenation of α-halo acyl halides, and dehydrohalogenation of acyl halides with tertiary amines in a solvent, are multistep processes with the utilization of hazardous reagents and solvents producing chlorinated byproducts.[20] Therefore, ketene production by the catalytic pyrolysis of carboxylic acids over silica is an environmentally benign alternative.[21] Thus, investigation of the catalytic pyrolysis mechanism of carboxylic acids over silica is essential for further developing oleochemical production methods.

Ketenes attract significant interest as synthons in organic synthesis due to their high reactivity and nucleophilicity.[17,22] Importantly, ketenes are considered privileged synthons in the syntheses of three-, four-, five-, and six-membered heterocycles.[23] They can be used to synthesize any organic acid derivatives and as acylating agents,[24] for example, in the catalytic acylation of anisole by acetic anhydride to yield *p*-methoxyacetophenone.[25,26] Ketenes are also used in pharmaceutical applications such as preparing β-lactam antibiotics.[27]

In addition, establishing the critical role of ketenes as an essential member of the highly reactive first-generation reaction intermediates such as carbocations, carbanions, radicals, and carbenes has been the target in a number of studies mainly during the last five years.[28−32] Their crucial role in processes of zeolite catalysis was identified as (1) syngas to light olefins over oxide−zeolite-based composites;[31] (2) methanol conversion to hydrocarbons;[29] (3) catalytic acylation of anisole by acetic anhydride to yield *p*-methoxyacetophenone;[25] (4) ketene transformation to gasoline;[30] (5) ketonization of aliphatic acids;[32] and (6) acid-catalyzed carbonylation over zeolites.[33] Chen and coauthors showed that ketenes are intermediates in the acid-catalyzed carbonylation over zeolites by *ab initio* molecular dynamics simulations and the confinement effect enforced by the pores of zeolites significantly influences this reaction (via formation and stability of ketenes[33]). The role of ketenes was revealed as a critical intermediate and product in the pyrolysis processes of biomass and its model compounds, i.e., cinnamic acids.[34,35]

The usage of a variety of quantum-mechanical methods, including density functional theory (DFT) to model silica surfaces was discussed by Rimola et al.[36] The established patterns of catalytic pyrolysis can help to select conditions of the process, inorganic oxides, to obtain the desirable product in quantitative yields. In addition, establishing binding mechanisms with the surface is practical in method development solving urgent problems in biology and medicine. Indeed, the carboxyl group is the primary building block of practically all essential biomolecules (amino acids, peptides, proteins, lipids, etc.). Although many studies investigate carboxylic acid decomposition on the silica surface, adsorption mechanisms, and the surface intermediates, these brought to date no clear conclusion. The influence of hydrophilic and hydrophobic interactions and hydrocarbon chain length on adsorption mechanisms could not be established as well as mechanisms of ketene formation on the silica surface and the influence of the structure of acids on them. Hence, an endeavor has been undertaken to investigate the kinetics and mechanisms governing chemical reactions involving carboxylic acids on the surface layer of silica materials. The objective is to ascertain the adsorption structures of the complexes formed and understand the underlying mechanisms in the interaction between substances containing a carboxyl group and active sites present on the silica surface.

## 2. EXPERIMENTAL SECTION

**2.1. Reagents.** Fumed silica A-300 (pilot plant at the Chuiko Institute of Surface Chemistry, Kalush, Ukraine; specific surface area of 270 $m^2 \cdot g^{-1}$) was used in this work. Fumed silica was previously heated on air for 2 h at 400 °C for removal of adsorbed organic substances. The aliphatic carboxylic acids were obtained from Merck, Germany (methanoic acid (formic), ethanoic acid (acetic), propanoic acid (propionic), butanoic acid (butyric), 2-methylpropanoic acid (isobutyric), pentanoic acid (valeric), hexanoic (caproic), octadecanoic acid (stearic), 99.5%), and Fluka, Germany (2,2-dimethylpropanoic acid (pivalic acid), 99.5%). Glyceryl trimyristate was obtained from Merck, Germany (≥99%). Rapeseed meal used in this work was obtained from the Kyiv region of Ukraine.

**2.2. Loading FAs on the Silica Surface.** *2.2.1. Equilibrium Adsorption Procedure.* A 100 mg portion of silica was immersed in an aqueous solution of suitable acid of the appropriate concentration (0.01−0.1 $mol \cdot L^{-1}$) at pH 3.2 ± 0.3 and stirred at room temperature for 24 h to achieve equilibrium. The suspension was decanted and centrifuged for 20 min at 10.000 rpm until the supernatant is clear. Then, samples were dried in air at room temperature. The samples were then aged at room temperature for 24 h, dried, and stored in a desiccator. An adsorption value was determined by difference in the aqueous phase concentration of the organic acids before and after adsorption. The concentration of acids in solutions has been determined by titration with NaOH solution using phenolphthalein as the indicator before and after adsorption.

The adsorption capacity of silica toward FAs in $mg \cdot g^{-1}$ was calculated as

$$q = \frac{(C_0 - C_{eq}) \times V}{m}$$

where $C_0$ and $C_{eq}$ correspond to the initial and equilibrium concentrations of FA, respectively, ($mg \cdot L^{-1}$); $V$ corresponds to the volume of the acid aqueous solution (mL); and $m$ corresponds to the mass of sorbent (g).

*2.2.2. Gas-Phase Adsorption.* Adsorption of acid molecules was provided by expanded vapors of pentanoic acid on the preliminary outgassed (450 °C, 133 Pa, 2h) thin self-supporting wafer $SiO_2$ sample. Prior to adsorption, pentanoic acid was degassed by online freeze−pump−thaw cycles performed at liquid nitrogen temperature.

*2.2.3. Modification by Impregnation.* Additionally, other samples with concentrations of 0.1, 0.3, 0.4, and 0.6 $mmol \cdot g^{-1}$ of the corresponding acid on the silica were obtained by impregnation. A 25 mL of aqueous solution of acid was added to 1 g of fumed silica in Petri dish. A sample of hexanoic acid due to its low solubility in water was obtained from aqueous ethanol solution (50% alcohol by volume) of silica. The silica-supported acid samples for thermogravimetric analysis were obtained by soaking silica in $CCl_4$ solutions of the corresponding acid. The stearic acid and glyceryl trimyristate samples (0.3 $mmol \cdot g^{-1}$) on the silica surface were obtained by soaking silica in their ethanol solutions. The components were mixed and left on air at ∼20 °C until the solvent was fully evaporated (∼24 h). Mechanical mixtures of rapeseed meal with silica were obtained by grinding in an agate mortar. In experiment, an air-dried sample was under investigation. The samples were then aged at room temperature for 24 h, dried, and stored in a desiccator.

**2.3. Fourier Transform Infrared Spectroscopy (FTIR).** FTIR-spectra were recorded at room temperature in the range between 400 and 4000 $cm^{-1}$ on a Thermo Nicolet NEXUS FT-IR spectrophotometer. The spectra were obtained with a theoretical resolution of 4 $cm^{-1}$ with 100 scans and a scan speed of 0.5 $cm \cdot s^{-1}$. FTIR spectra were obtained for all samples (adsorbed and impregnated). Both the self-supporting discs (pellets) prepared by pressing, using 8 MPa pressure, weighing about 20 mg, and the powder weighing about 180 mg were used in the IR spectrometric measurement. The weights of silica samples were 20 (for pellets) and 180 mg (for powder).

Pellets of silica-supported acids with a density of 2−3 $mg \cdot cm^{-2}$ for FTIR investigations with heating and evacuation steps were placed in a specially designed cell attached to the vacuum system. The cell was


https://doi.org/10.1021/jacs.3c06966
J. Am. Chem. Soc. XXXX, XXX, XXX−XXX

designed in way allowed carry out heating and further evacuation without change arrangement of sample in the cell. The sample was evacuated at room temperature and a pressure of $10^{-4}$ mmHg for 3 h before measurements. Spectra were taken after evacuation at room temperature and 60 and 100°C on a Specord-75 IR spectrometer ("Carl Zeiss", Germany).

**2.4. *In Situ* IR Spectroscopy.** A heatable and stationary mounted quartz glass IR cell equipped with cooled KBr windows was used for the examination of adsorbed species produced as a result of surface reactions of valeric acid molecules on the active centers of $SiO_2$ following a temperature treatment at desired temperatures. Specord IR-75 ("Carl Zeiss", Germany) was the employed spectrometer. The spectra were recorded after outgassing samples at the desired temperature (kept for 5 min) and cooling to RT. For these studies, samples of pentanoic acid obtained by adsorption from the gas phase and by the impregnation method (0.3 mmol·g$^{-1}$) were used.

**2.5. Method of Temperature-Programmed Desorption Mass Spectrometry.** The method of conducting the TPD MS experiment was described in detail in a number of our previous publications,[37−39] as well as obtaining kinetic parameters from the TPD MS data.[38,39]

**2.6. Thermogravimetric Analysis.** Thermogravimetric analyses of samples were run on a thermogravimetric analyzer TGA-6 (PerkinElmer, USA) in an oxygen atmosphere (flow rate = 20 cm$^3$·min$^{-1}$). In a typical run, 20 mg of the sample was heated from 30 to 700°C at a heating rate of 10°C·min$^{-1}$.

**2.7. Quantum Chemical Methods.** The density functional theory method (DFT) was used to identify the nature of the absorption bands in the IR spectra. DFT calculations were carried out using the B3LYP, wB97XD, and M062X functionals and the 6-311++G(d,p) basis set. The last two functionals include the dispersion correction of forces, which is especially important in the study of intermolecular interactions. All calculations were performed using the GAUSSIAN 09 software (version D.01).[40] Active centers of the silica surface on which the adsorption and further thermal transformations of valeric acid probably occur were selected within[41] the framework of the cluster approximation model. In this approximation, the broken chemical bonds at the silica active centers, directed into the volume of the solid, were closed by hydrogen atoms.

In addition, the silica surface itself was modeled using two different approaches. The first one is based on the "soft" surface model, in which the $SiO_4$ fragments in the active center can move relatively easily relative to each other. In this case, the structural rigidity (the possibility of rearrangement) is determined mainly by the energies of hydrogen bonds and dispersive interactions. The second approach is the so-called "hard" surface model. The possibility of the active center reorganization is determined primarily by the deformation of Si−O−Si and O−Si−O valence angles and the change in the torsion angles between its fragments.

## 3. RESULTS AND DISCUSSION

Establishing the interaction between the silica surface and compounds containing a carboxyl group is of significant fundamental and applied importance. Ketenization reaction kinetics for a series of aliphatic acids on a silica surface was previously investigated using the linear free energy relationships (LFER) approach.[19] Kinetic parameters and reaction constants, $\rho_0$, were calculated for the reaction of ketene formation. Based on the data obtained, an intramolecular mechanism of ketenization was proposed from an adsorbed carboxylate, which proceeds through a four-membered low-polarity transition state. However, the question regarding the adsorbed carboxylate remains open mainly because there is no sufficient spectroscopic confirmation of such species, e.g., the corresponding IR absorption bands. Despite surface siloxane bonds being nonactive,[19,38] silanol groups lead to carboxylates upon interaction with the acidic substrate leading to an absorption band $\nu_{C=O}$ around 1680 cm$^{-1}$ for adsorbed valeric acid.[15,21,42,43] An alternative adsorption mechanism was proposed resulting from a nucleophilic addition to siloxane bridges.[19,35] Zhuravlev[44] considers the formation of reactive siloxane bridges resulting from surface dehydration and dehydroxylation processes as confirmed in several simulation works.[45] These studies provide data on the participation of siloxane bridges in nucleophilic addition reactions, particularly with ammonia and some primary, secondary, and tertiary amines.[46] The data of TPD MS studies[19] indicate a more complex nature of the interaction of aliphatic acids with the silica surface. In particular, three stages of desorption and destruction of carboxylic acids from the surface indicate at least three surface forms of adsorption. Obviously, the silica surface cannot be described only by the ideal cristobalite structure with uniformly distributed silanols; i.e., the surface may present areas of unevenly distributed silanol groups and hydrophobic siloxane. The following IR spectroscopy adsorption data and computational simulations correlate the stages during the pyrolytic process to specific adsorption modes of carbolylic structures on silica surfaces, including forming donor−acceptor intermediate complexes between the carboxylic substrates and a penta-coordinated silicon atom.

**3.1. Adsorption Properties.** The carboxylic substrates' adsorption data (Figures 1 and 2 and Table 1) is well

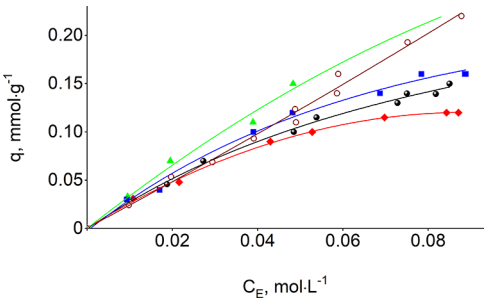


**Figure 1.** Adsorption isotherms of methanoic acid (circle solid), ethanoic acid (red tilted square solid), propanoic acid (green triangle up solid), butanoic acid (blue box solid), pentanoic acid (circle open) on the silica surface from aqueous solution.

described by the Langmuir isotherm model ($R^2$ = 0.9534−0.9897), leading to an L-shape for adsorption isotherms of linear acid isomers and an S-shape for branched-chain isomers. Values of equilibrium adsorption capacity ($q_{max}$), adsorption equilibrium constant ($K$), and Gibbs free energies ($\Delta G$) were obtained from linear regression analysis of known Ce and $q$

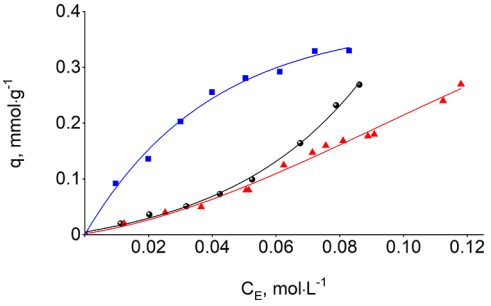


**Figure 2.** Adsorption isotherms of 2-methylpropanoic acid (circle solid), 2.2-dimethylpropanoic acid (red triangle up solid), and hexanoic acid (blue box solid) on the silica surface from aqueous solution.


https://doi.org/10.1021/jacs.3c06966
J. Am. Chem. Soc. XXXX, XXX, XXX−XXX

**Table 1. Physico-Chemical Parameters of Adsorption of Carboxylic Acids on the Silica Surface (Obtained by Linear Regression Analysis for Langmuir Adsorption Isotherm)**

| acid | $q_{max}$/ mmol·g$^{-1}$ | K/L·mol$^{-1}$ | $\Delta G$/ kJ·mol$^{-1}$ | $R^2$ |
|---|---|---|---|---|
| methanoic (formic) | 0.36 | 8.02 | −4.73 | 0.9860 |
| ethanoic (acetic) | 0.21 | 15.7 | −6.2 | 0.9897 |
| propanoic (propionic) | 0.42 | 9.2 | −5.0 | 0.9891 |
| butanoic (butyric) | 0.28 | 6.6 | −4.3 | 0.9846 |
| pentanoic (valeric) | 0.33 | 6.9 | −4.4 | 0.9534 |
| 2,2-dimethylpropanoic (pivalic) | 0.25 | 1.61 | −1.1 | 0.9879 |
| hexanoic (caproic) | 0.50 | 22.3 | −7.04 | 0.9807 |

values[47,48] and are listed in Table 1. The equilibrium adsorption capacities, proportional to the concentration of free silanol groups on the fumed silica surface (0.6 mmol·g$^{-1}$), expand between 0.2 and 0.5 mmol·g$^{-1}$. The isotherm-derived Gibbs free energies for propanoic, butanoic, and pentanoic acids have very close values, indicating a low affinity between carboxylic acids to the silica surface.

**3.2. FT-IR.** *3.2.1. FT-IR Investigation of Carboxylic Acids Adsorbed on the Silica Surface from the Aqueous Phase.* Upon silica exposure to the carboxylic substrates, FT-IR spectra were investigated in order to determine the adsorption modes and the complexes' structure. The observed vibration of the carboxylic $\nu_{C=O}$ stretching in saturated fatty acids is more intense than in ketones, appearing in the 1725−1705 cm$^{-1}$ range (Table 2). These are comparatively lower to isolated saturated aliphatic acids in inert solvents (1760 cm$^{-1}$) due to the hydrogen bonds formed between carboxylic acid dimers.[49] No bands could be attributed to unassociated carbonyl groups, typical monomeric acids, on samples obtained by the impregnation method (0.2−0.5 mmol·g$^{-1}$). The absence of any vibration bands at 1760 cm$^{-1}$ suggests that carboxylic acid is not free but rather associated. Indeed, the intensity of stretching vibrations of isolated silanols at 3745 cm$^{-1}$ decreased for all investigated acids, confirming the formation of hydrogen-bonded adsorbed complexes SC II (Scheme 1). The stretching band at 3745 cm$^{-1}$ did not completely disappear (Figure 2), meaning that not all isolated silanols (∼20%) participate in the formation of adsorption complexes with carboxylic acids. The dependence of surface coverage versus acid surface concentration was calculated from the band's intensity for hexanoic and propanoic acids. Ca. 20% of silanols formed the surface complex even at high surface coverage.

A $\nu_{C=O}$ frequency blue-shift (higher frequencies) relative to dimer stretching of $\Delta\nu_1$ = 21 cm$^{-1}$ ($\Delta\nu_1 = \nu_{dimer} - \nu_{ads.ac.}$) is observed for hexanoic acid, opposite to the red-shift of $\Delta\nu_1$ = 34 cm$^{-1}$ for propanoic acid (Table 2).

A shift to higher frequency indicates the formation of hydrogen-bonded adsorbates SC II (Scheme 1) due to the weaker hydrogen bond between silanol groups (Scheme 1); red-shifts point toward the suggested formation (Scheme 1; SC IIIa, SC IIIb). Indeed, considering the $\nu_{(C=O)}$ shift ($\Delta\nu_2 = \nu_{monom.} - \nu_{ads.ac.}$) relative to monomeric carboxylic acid at 1757 cm$^{-1}$, it is possible to assign, for instance, the hexanoic acid $\nu_{C=O}$ bands to $\Delta\nu_{2C=O}$ = 71 cm$^{-1}$ − adsorption complex SC IIIa (the Scheme 1); $\Delta\nu_{2C=O}$ = 54 cm$^{-1}$ − adsorption complex SC IIIb (Scheme 1); $\Delta\nu_{2C=O}$ = 41 cm$^{-1}$ − dimer of acid SC I (Scheme 1); $\Delta\nu_{2C=O}$ = 25 cm$^{-1}$ − hydrogen-bonded complex SC II (Scheme 1). Similarly, the $\nu_{C=O}$ stretching band for the adsorbed butanoic acid sample is suggested to deconvolute in three interactions, whereas they are four for adsorbed propanoic and hexanoic acid samples (Figures 3 and 4 and Table 2). Such IR band deconvolution of silica-adsorbed species is explained by various adsorption complexes, as previously reported for carboxylic acids, ketones, and esters.[47,50] The most characteristic vibrational bands corresponding to surface complexes SC IIIa,b are at 1697−1705 cm$^{-1}$, corresponding to low and high coverages (Figures S1 and S2 (Supporting Information)). While similar shifts of the bands of carbonyl group $\nu_{C=O}$ were observed for all carboxylic acids, Table 2 presents data specifically for hexanoic acid in order to illustrate the aforementioned discussion.

*3.2.2. In situ IR Study of Valeric Acid Conversion over Silica obtained from Gas Phase and by Impregnation from Aqueous Solution.* The IR of pentanoic acid on silica shows a relevant band at 1685 cm$^{-1}$ corresponding to surface complexes SC IIIa,b and can be observed under various conditions: room temperature and atmospheric pressure and after evacuation in vacuum at 20, 60, and 100 °C (Figure 4). While the intensity of such band remains upon evacuation in a vacuum, the vibration related to physically adsorbed water at 1621−1631 cm$^{-1}$ significantly decreases (although still observable under vacuum at 100 °C due to the hydroxyl groups on the surface). The vibrational band at 1621−1631 cm$^{-1}$ in the FTIR spectrum is attributed to the combined contributions of strongly bound water within voids and physically adsorbed water on the silica's surface. While the band's intensity remains upon evacuation in a vacuum due to the presence of strongly bound water within voids, the hydroxyl groups on the surface allow for the continued

**Table 2. Absorption Frequencies of the Carbonyl Group $\nu_{(C=O)}$ for Silica-supported Samples of Hexanoic Acid and Corresponding Shift Values $\Delta\nu_{(C=O)}$ Relative to $\nu_{(C=O)}$ of Monomer and Dimer[a]**

| sample of acid | acid solution in $CCl_4$ (monomer)[49] | acid solution in $CCl_4$ (dimer)[49] | acid adsorbed on the silica surface from aqueous solution | | | acid immobilized on the silica surface by impregnation (0.6 mmol·g$^{-1}$) | | |
|---|---|---|---|---|---|---|---|---|
| | $\nu_{C=O}$, cm$^{-1}$ | $\nu_{C=O}$, cm$^{-1}$ | $\nu_{C=O}$, cm$^{-1}$ | $\Delta\nu_1$, cm$^{-1}$ | $\Delta\nu_2$, cm$^{-1}$ | $\nu_{C=O}$, cm$^{-1}$ | $\Delta\nu_1$, cm$^{-1}$ | $\Delta\nu_2$, cm$^{-1}$ |
| hexanoic (caproic) 0.503 mmol·g$^{-1}$ | 1757 | 1711 | 1686 | +25 | +71 | 1685 | +26 | +72 |
| | | | 1703 | +8 | +54 | 1705 | +6 | +52 |
| | | | | | | 1716 | −5 | +41 |
| | | | | | | 1732 | −21 | +25 |

[a]$\Delta\nu_1 = \nu_{dimer} - \nu_{ads.}$ − absorption frequencies, $\nu_{C=O}$ shift of adsorption complex relative to the dimer. $\Delta\nu_2 = \nu_{monomer} - \nu_{ads.}$ − absorption frequencies, $\nu_{C=O}$ shift of adsorption complex relative to monomer.



https://doi.org/10.1021/jacs.3c06966
J. Am. Chem. Soc. XXXX, XXX, XXX−XXX

**Scheme 1. Surface Complexes of Carboxylic Acids on the Silica Surface**[a]

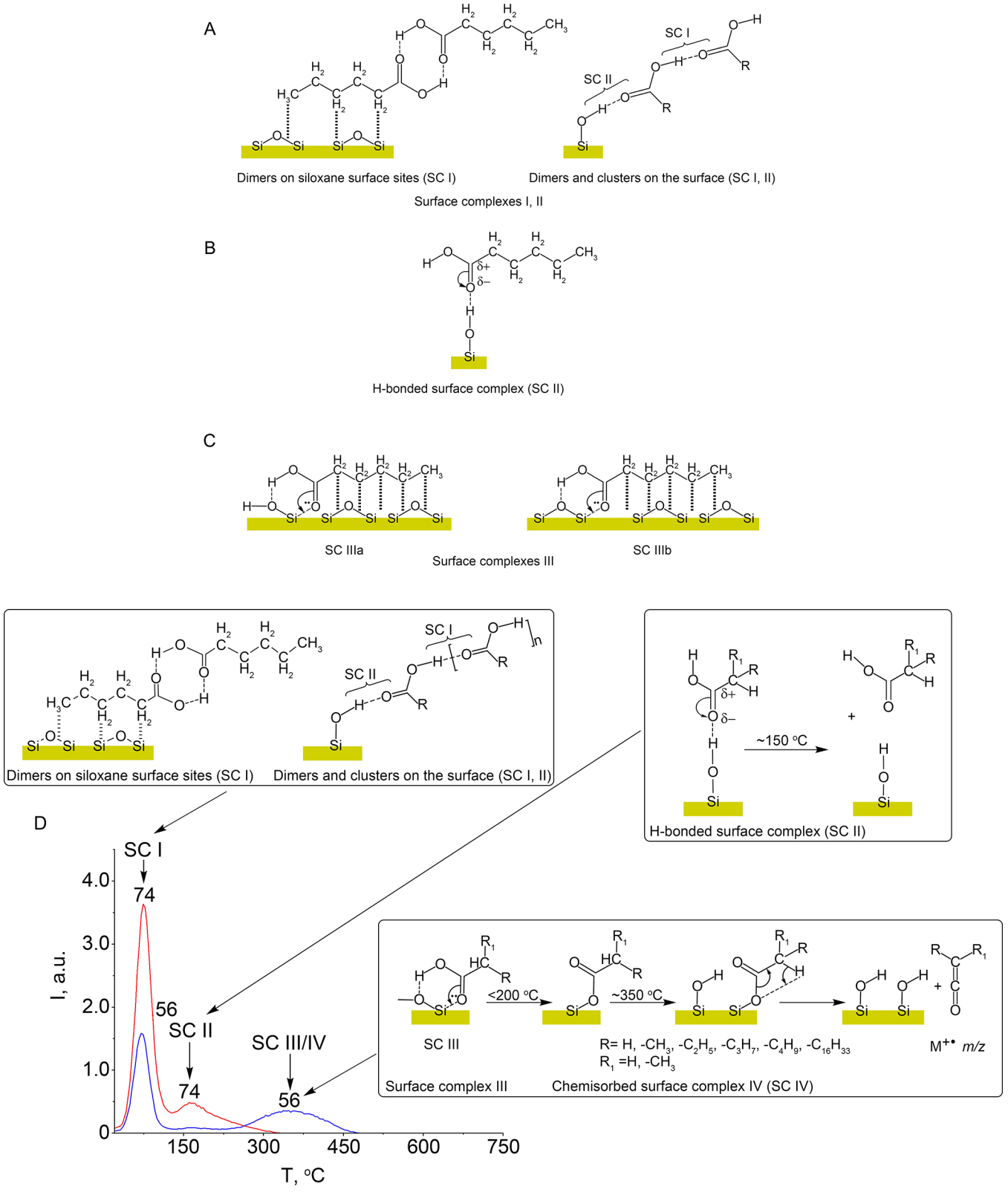


[a](A) dimers and clusters, physically adsorbed complexes of acid, SC I; (B) hydrogen-bonded complexes SC II; (C) donor−acceptor coordination complexes SC IIIa and SC IIIb. (D) TPD-peaks related to the thermal decomposition of the surface complexes SC I, SC II, SC IIIa, and chemosorbed complex SC IV, which decomposes with ketene formation.

observation of the band related to physically adsorbed water, even at elevated temperatures under vacuum conditions.

Monodentately bound complexes of fatty acids on the surface of silica are challenging to identify employing IR



https://doi.org/10.1021/jacs.3c06966
J. Am. Chem. Soc. XXXX, XXX, XXX−XXX

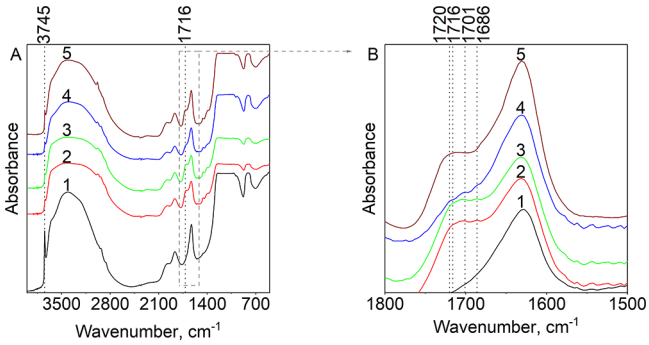


**Figure 3.** IR-spectra in the range of (A) 4000−400 and (B) 1800−1500 $cm^{-1}$ of silica (line 1) and silica-supported acids (adsorbed): hexanoic (0.503 mmol·$g^{-1}$; line 2), pentanoic (0.327 mmol·$g^{-1}$; line 3), butanoic (0.282 mmol·$g^{-1}$; line 4), and propanoic (0.42 mmol·$g^{-1}$; line 5).

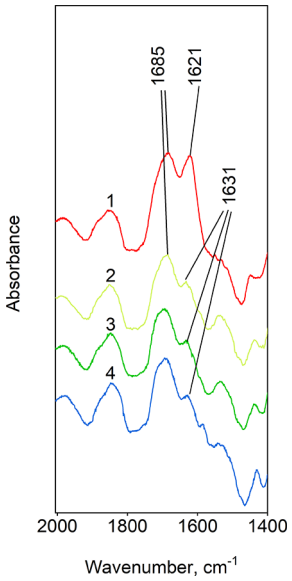


**Figure 4.** *In situ* IR spectroscopy. IR spectra of pentanoic acid on the surface of $SiO_2$ (0.3 mmol·$g^{-1}$): (1) at room temperature; (2) after evacuation; (3) after heating to 60 °C; and (4) after heating to 100 °C.

spectroscopy since their $\nu_{C=O}$ absorption region at ∼1680 $cm^{-1}$ is overlapped with the $\nu_{C=O}$ band (∼1715−1730 $cm^{-1}$) and the water $\delta_{(H-O-H)}$ band at 1640 $cm^{-1}$. However, the latest band significantly shifts toward low wavenumbers with increasing strength of interaction of water molecules with the surface.[51] In addition, silica overtones are known to be located at 1640, 1870, and 1960 $cm^{-1}$.[52] Monodentate bound complexes of fatty acids were identified through vibrational analysis ($\Delta\nu = \nu_{C=O} - \nu_{C-O}$) for several nanosized oxides.[15] For silica, $\Delta\nu$ is 285 $cm^{-1}$ and corresponds to monodentate complexes.[53] Based on this and to clarify the mechanisms of interaction of fatty acids with the silica surface, the thermal evolution of the absorption bands in the range of 1400−1900 $cm^{-1}$ for pentanoic acid adsorbed from the gas phase was subsequently investigated. The sample heating temperature range was chosen based on our previous studies. Thermal transformations of pentanoic acid on the surface of silica end at ∼450 °C (Figure 5) as TPD curves of molecular and fragment ions of propylketene show that the desorption of propylketene drops to zero at ∼450 °C.[15,19] At this temperature, the absorption disappears in the region corresponding to $\nu_{C-O}$ and deformation vibrations $\delta_{C-H}$ of $CH_2$ and $CH_3$ groups. This result is consistent with the TPD MS data and confirms the absence of any pentanoic acid on the silica surface at temperatures above 450 °C.

The formation of a much smaller number of dimers and associates on the surface is observed compared to adsorption from the aqueous phase during adsorption from the gas phase (Figure 5). This is evidenced by the decrease in absorption intensity at ∼1720 $cm^{-1}$, which is observed in the spectra in Figure 5 as compared to those in Figure 4. The intensity of the absorption band at 1680 $cm^{-1}$ became almost the same as the intensity of the absorption band of water $\delta_{H-O-H}$, since the intensity of the latter decreased due to vacuuming and the fact that adsorption was carried out by the gas-phase method and not from an aqueous solution. However, applying the gas phase adsorption technique did not allow for achieving a clear separation of absorption in the region of ∼1720−1610 $cm^{-1}$ into individual components.

The IR absorption corresponding to $\nu_{C=O}$ is present as a shoulder on the water absorption band. Regardless, studying the thermal evolution of these bands from room temperature to 400°C revealed a divergence of two peaks at ∼1615 and ∼1640 $cm^{-1}$, Figure 5. The shift related to the water $\delta_{H-O-H}$ bending vibration is related to an increase in the strength of the interaction of the water molecule with the surface.[51] Furthermore, Schnetzer showed that the lower wavenumber of $\delta_{(H-O-H)}$ is observed for water molecules in a highly polarized state.[51]

The strongest interaction of water molecules with the surface of silica is observed at ∼200 °C since; at this temperature, the lowest value $\lambda_{max}$ of the absorption band of the bending vibration of water $\delta_{H-O-H}$ was recorded, Figure 6. Upon further heating to 400 °C, no additional shift to lower wavenumbers was observed. No splitting of the water band is observed at 450 °C. This implies that all forms of water, including any associated components, have disappeared upon decomposition at this temperature.

The investigation of pentanoic acid on silica revealed the presence of two distinct forms of water: strongly bound water, which is associated with adsorption complexes, and weakly bound water. Notably, the behavior of water desorption during the temperature-programmed desorption (TPD) process is different, with a significant decrease in the intensity of water desorption observed specifically at the temperature of ketene desorption (∼360 °C). The bands at ∼1636 ($\delta_{H-O-H}$) and ∼1860 $cm^{-1}$ (silica overtone) are often used to provide a semiquantitative elucidation of adsorbed water content in the surface layer.[54] However, they overlap, making an accurate measurement of their areas challenging, Figure 7. From the similar intensities of these bands, one can suggest approximately the same amount of each form. The intensity ratio of these two bands decreased with increasing temperature until 200 °C, Figure 7. At this temperature, it reaches a plateau, and at 450 °C, it gets a value of ∼0.6, which is consistent with literature data for silica materials. Costa et al.[54] showed that the ratio between the areas of the 1636 and 1860 $cm^{-1}$ bands does not reach zero because the absorbance area at the 1636 $cm^{-1}$ band includes an overtone of silica at ∼1640 $cm^{-1}$.

**3.3. Quantum Chemical Calculations.** Table 3 shows the wavenumbers related to the normal vibrational modes of adsorbed complexes on silica. During analysis of the simulated results, special attention was dedicated to identifying the


https://doi.org/10.1021/jacs.3c06966
J. Am. Chem. Soc. XXXX, XXX, XXX−XXX

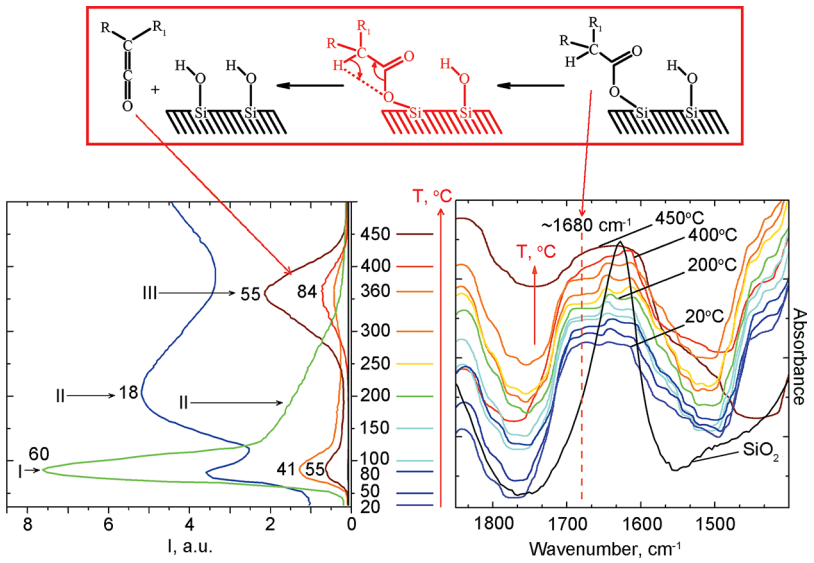


**Figure 5.** *In situ* IR spectroscopy and TPD-curve for molecular and fragment ions of propylketene ($m/z$ 84, 55, 41), fragment ions of valeric acid ($m/z$ 60, 55, 41), and molecular ion of water ($m/z$ 18) obtained during pyrolysis of valeric acid over nanosilica.

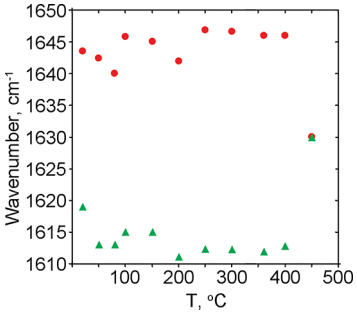


**Figure 6.** Thermal evolution of the absorption band of the bending vibration of water $\delta_{(H-O-H)}$.

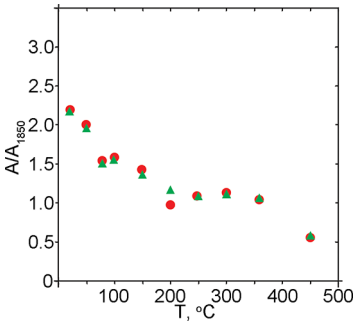


**Figure 7.** Thermal evolution of the ratio between the intensities of the bending vibration of the water $\delta_{(H-O-H)}$ band and the silica overtone band (~1840−1850 $cm^{-1}$). Red − $A_{1640/1850}$ (weakly bound water); green − $A_{1615/1850}$ (strongly bound water).

carboxyl group vibrations of valeric acid and its anion (Figure 8). We measured the shift of wavenumbers characteristic of the different surface complexes and associated them with the structural rigidity of the selected models and interacting atoms.

The band at 1680 $cm^{-1}$ was assigned to the vibrations of the dissociated carboxyl group, as the simulated IR bands agree with the experiments. The band corresponds to the bond between the carboxyl oxygen and the surface silicon atom, which becomes pentacoordinate (Figure 9). As the data in Table 3 show, this obtained result does not depend on the "soft" or "hard" model of the silica surface. However, it is determined only by the reactivity of the pentanoic acid molecule itself and the coordination capabilities of the silicon atoms on the surface. The formation of such a surface complex was also shown by Abdallah and coauthors.[55] Additionally, the existence of two types of water in the IR spectra until the complete conversion of acid into ketene provides additional evidence of the bonding of acids with strained siloxane bridges.[44]

Figure 8 schematically shows all types of adsorption complexes obtained as a result of DFT modeling. Table 3 shows the values of the total energies ($E_{tot}$) of all these complexes calculated by the DFT method as well as the values of the highly characteristic frequencies of the carboxyl group of pentanoic acid or its anion and the intensity of these frequencies.

Analysis of $E_{tot}$ values (Table 3) for all structures shown in Figure 8 allowed us to conclude that for structures of the A1−A10 group; the energetically most favorable structures are those in which pentanoic acid or its anion binds to the silica cluster through hydroxyl groups. The situation is different for the "hard" surface model, structures B1−B7. The difference is that in the case of an anion of an acid, this form of adsorption becomes energetically more favorable (Figure 8, structure B5), when the carboxyl group directly interacts with one of the silicon atoms of the surface. With this type of interaction, silicon becomes penta-coordinated. For example, for the M062X functional, the B5 structure is 5.02 kcal·$mol^{-1}$ (preferable to B3 where intermolecular bonding occurs due to hydrogen bonds).

Figure 9 shows a summary of basic geometric parameters for all surface complexes where penta-coordinated silicon is formed. The magnitudes of the orders of coordination bonds between the oxygen of the carboxyl group and the corresponding silicon on the silica surface are also indicated. Such values of bond orders unambiguously confirmed the formation of penta-coordinated silicon.

Structure C1 is a surface complex formed by hydrogen bonds. The bond lengths (functional M062X) are indicated in Angstroms, and in parentheses are the bond orders obtained


https://doi.org/10.1021/jacs.3c06966
J. Am. Chem. Soc. XXXX, XXX, XXX−XXX

Table 3. Values of Total Energy and Normal Vibrations Calculated by the DFT Method for Complexes of the Silica Surface with a Neutral Molecule and an Anion of Pentanoic Acid, which Are Different in Nature, See Figures 8 and 9[a]

| structure | acid molecule state | functional | total energy ($E_{tot}$), au | frequency, $cm^{-1}$ | IR intensity, (km/mol) |
|---|---|---|---|---|---|
| A1* | anion | B3LYP | −2489.834440 | 1620 | 853.49 |
| | | wB97XD | −2489.328791 | 1683 | 543.45 |
| | | M062X | −2489.236709 | 1697 | 560.08 |
| A2 | neutral | B3LYP | −2490.347200 | 1775 | 414.35 |
| | | wB97XD | −2489.831432 | 1815 | 449.48 |
| | | M062X | −2489.735112 | 1817 | 367.45 |
| A3 | neutral | B3LYP | −2490.347263 | 1769 | 404.37 |
| | | wB97XD | −2489.829392 | 1811 | 328.21 |
| | | M062X | −2489.737514 | 1823 | 335.74 |
| A4 | neutral | B3LYP | −2490.341615 | 1768 | 311.33 |
| | | wB97XD | −2489.830188 | 1815 | 327.57 |
| | | M062X | −2489.728803 | 1828 | 324.86 |
| A5 | neutral | B3LYP | −2490.345190 | 1756 | 316.68 |
| | | wB97XD | −2489.827023 | 1800 | 336.59 |
| | | M062X | −2489.727780 | 1817 | 343.18 |
| A6 | anion | B3LYP | −2489.847899 | 1595 | 653.78 |
| | | wB97XD | −2489.332636 | 1656 | 678.70 |
| | | M062X | −2489.236515 | 1660 | 654.12 |
| A7 | neutral | B3LYP | −2490.338512 | 1725 | 567.37 |
| | | wB97XD | −2489.825515 | 1771 | 569.46 |
| | | M062X | −2489.728725 | 1780 | 583.77 |
| A8 | anion (pentacoordinate Si) | B3LYP | −2489.824059 | 1688 | 402.06 |
| | | wB97XD | −2489.312576 | 1743 | 392.33 |
| | | M062X | −2489.227235 | 1753 | 376.40 |
| A9 | anion (pentacoordinate Si) | B3LYP | −2489.828675 | 1653 | 364.84 |
| | | wB97XD | −2489.314982 | 1707 | 394.75 |
| | | M062X | −2489.229216 | 1717 | 391.56 |
| A10 | neutral (pentacoordinate Si) | B3LYP | −2490.327281 | 1725 | 606.97 |
| | | wB97XD | −2489.817746 | 1763 | 617.02 |
| | | M062X | −2489.726480 | 1768 | 669.66 |
| B1** | anion (pentacoordinate Si) | B3LYP | −4174.238445 | 1661 | 522.59 |
| | | wB97XD | −4173.475992 | 1716 | 523.87 |
| | | M062X | −4173.407924 | 1684 | 591.30 |
| B2 | anion (pentacoordinate Si) | B3LYP | −4174.239087 | 1669 | 424.45 |
| | | wB97XD | −4173.476429 | 1718 | 433.03 |
| | | M062X | −4173.408024 | 1690 | 500.60 |
| B3 | anion | B3LYP | −4174.255982 | 1615 | 910.04 |
| | | wB97XD | −4173.484618 | 1671 | 866.49 |
| | | M062X | −4173.405767 | 1650 | 1102.22 |
| B4 | neutral | B3LYP | −4174.760011 | 1769 | 494.35 |
| | | wB97XD | −4173.993678 | 1810 | 443.49 |
| | | M062X | −4173.908980 | 1828 | 564.18 |
| B5 | anion (pentacoordinate Si) | B3LYP | −4174.247630 | 1652 | 428.52 |
| | | wB97XD | −4173.484559 | 1709 | 462.03 |
| | | M062X | −4173.413773 | 1721 | 474.98 |
| B6 | neutral | B3LYP | −4174.756579 | 1757 | 317.00 |
| | | wB97XD | −4173.987810 | 1803 | 334.50 |
| | | M062X | −4173.904618 | 1817 | 340.18 |
| B7 | neutral | B3LYP | −4174.759136 | 1769 | 469.31 |
| | | wB97XD | −4173.996225 | 1795 | 377.56 |
| | | M062X | −4173.910895 | 1813 | 401.69 |
| C1*** | anion | M062X | −6756.344541 | 1632 | 645.66 |
| C2 | anion (pentacoordinate Si) | M062X | −6756.355978 | 1718 | 469.13 |

[a]Only the values of the frequencies of highly characteristic oscillations where the carboxyl group of pentanoic acid or its anion participates are given. Frequencies were scaled by 1.0. *, Structures of the A series refer to the "soft" surface model. **, B series structures refer to the "hard" surface model. ***, C series structures refer to the extended "hard" surface model (Figure 9).

from the theory of natural bond orbital analysis, using NBO version 3.[56]

This highly relevant result confirmed the hypothesis of the formation of penta-coordinated silicon, with additional DFT



https://doi.org/10.1021/jacs.3c06966
J. Am. Chem. Soc. XXXX, XXX, XXX−XXX

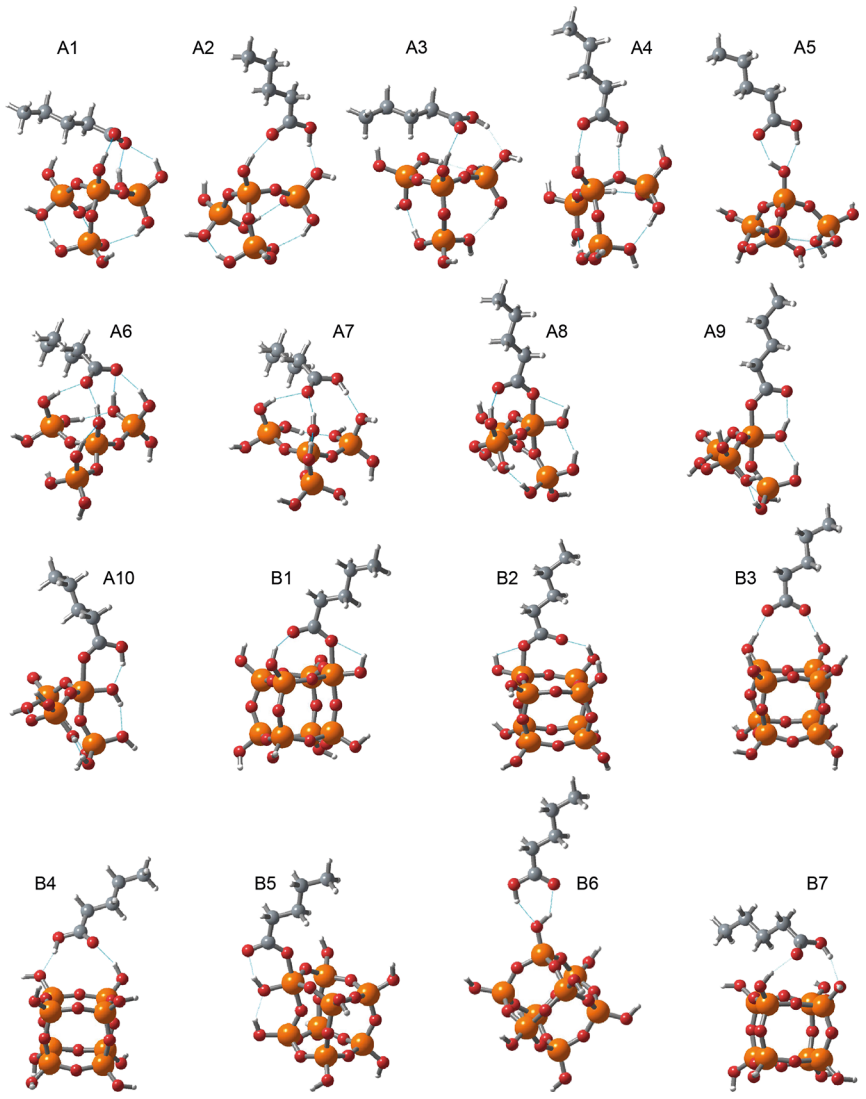


**Figure 8.** Structural types of surface complexes obtained from DFT calculations.

studies carried out for the extended model of the "hard" surface. Based on the extended model of the "hard" surface, the results on the formation of pentacoordinate silicon as a result of the adsorption of pentanoic acid anion on the structures of group B were fully confirmed. In addition, the lengths of the coordination bond between the oxygen of the carboxyl group and the surface silicon became significantly smaller (Figure 9) and the values of the bond orders became larger. These results further support the fact that the extension of the surface model led to even more favorable complexes with penta-coordinated silicon. Here it is appropriate to emphasize once again that only structures with penta-coordinated silicon can explain the presence of a band in the region of 1680 $cm^{-1}$ in the experimental IR spectra of pentanoic acid adsorption.

**3.4. Temperature-Programmed Desorption-Mass Spectrometry (TPD-MS) of Carboxylic Acids.** The high-temperature peak III was observed on TPD-MS curves for ions of hexadecyl ketene with $m/z$ 42, 55, 56, 70, 84, 98, 112, and 126 (Figure 10). These peaks describe the formation of ketenes upon desorption of octadecanoic acid fragments. It is known that the most intensive ion in the electron impact ionization (electron bombardment ionization, formerly known as electron impact) mass spectra of ketenes is the ion with $m/z$ 55 $[H_2C{=}C{=}C{=}O{-}H]^+$.[57] Peaks related to the destruction of chemisorbed fragment of acids with formation of ketenes $[CH_3(CH_2)_n{-}(H)C{=}C{=}O]^+$ (for ethanoic acid $CH_2{=}C{=}O$) where $n = 0{-}3$; 15 occur on the TPD curve of all saturated aliphatic carboxylic acids. The intensity of ions for this homologous series decreases with increasing molecular mass. An increase in hydrophobicity led to the formation of more surface complexes, and more ketenes developed. This result indicates that the pyrolysis pattern of low molecular weight aliphatic carboxylic acids on the silica surface is also typical for heavier acids. Therefore, this reaction seems to be universal and can be used to process plant raw materials, producing oleochemicals and bulk chemicals for organic synthesis.

Furthermore, data from earlier studies demonstrated that during pyrolysis of carboxylic acids on silica within a homologous series, a direct correlation is present between the maximum acid decomposition temperature with ketene release, and both length and branching of the acid chain.[19,43,58] Specifically, a longer and more branched acid chain corresponds to a higher decomposition temperature. Interestingly, if such a trend is not exclusive to carboxylic acids, this could imply a possibility to extend such patterns to biomass/waste pyrolysis, particularly those with significant triglyceride


https://doi.org/10.1021/jacs.3c06966
J. Am. Chem. Soc. XXXX, XXX, XXX−XXX

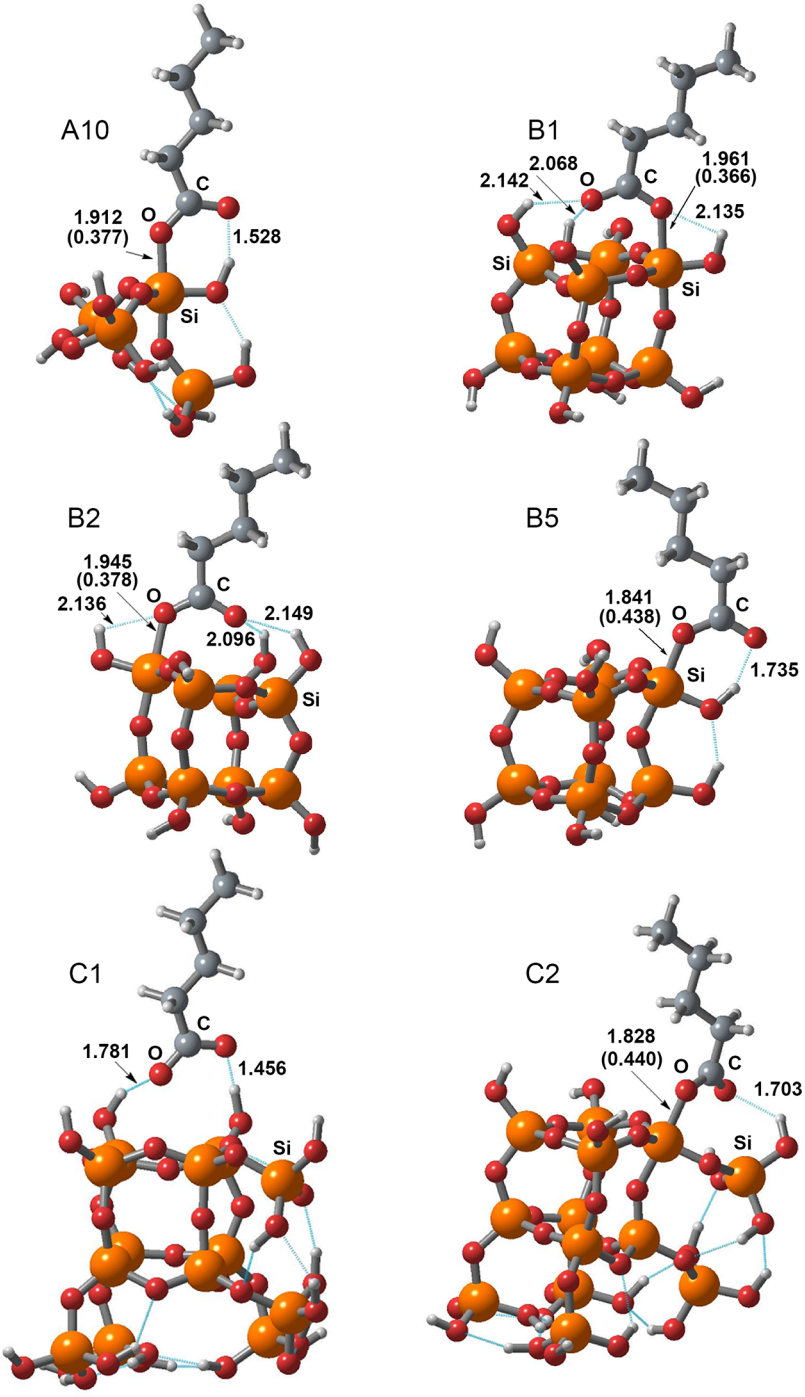


**Figure 9.** Molecular models for carboxylic acid species adsorbed onto the silica model via the pentacoordinate silicon surface atom.

fatty acid content. However, it is pertinent to note that Libby et al.'s study did not determine a relationship between chain length and activation energy required for ketene evolution.[21]

The ratio between peak intensities increases in homologous series, although uncorrelated with the substate's acidity, since the p$K_a$ remains practically constant over the entire range of compounds studied (Table 3). A shift of the $\nu_{C=O}$ absorbance band of more than 60 cm$^{-1}$ to the low-frequency region takes place as compared to that of the monomer ($\nu_{C=O}$ = 1757 cm$^{-1}$), and a low perturbation degree of free surface silanols (surface coverage $\theta \approx 0.2$) testifies favorably to the formation of the surface-adsorbed complex bonded with a bond stronger than hydrogen. Such additional evidence confirms that the acid adsorption on silica occurs via forming a donor−acceptor complex, i.e., n-electrons of the carbonyl's oxygen bonds with empty Si d-orbitals, which is more favorable with increasing the aliphatic chain length[62] because this increasing chain length results in increasing electron density on the oxygen atom of the C═O bond. Considering the increase in hydrophobicity, it is observed that the intensity of the ketene peak, observed based on octadecanoic acid, also increases. This correlation suggests that the number of complexes formed on the surface increases with an increase in hydrophobicity. Therefore, the intensity of the ketene peak can serve as an indicator of the enhanced


https://doi.org/10.1021/jacs.3c06966
J. Am. Chem. Soc. XXXX, XXX, XXX−XXX

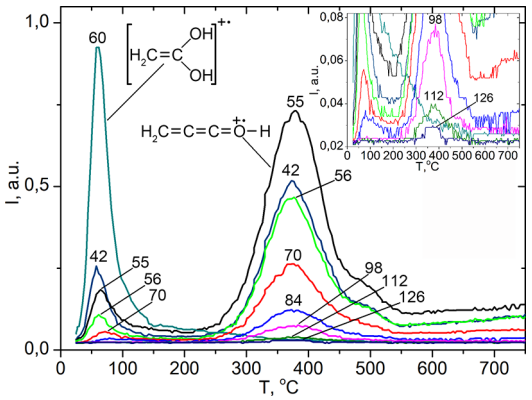


**Figure 10.** Pyrolysis of silica-supported octadecanoic (stearic) acid (0.3 mmol·g$^{-1}$). TPD curves of fragment ions of the molecular ion of octadecanoic acid with $m/z$ 60 (the most intense ion in the MS spectra of aliphatic acids), 42, 55, 56, 70, and 84 attributed to the desorption of the physically adsorbed acid. TPD curves of the fragment ions of the hexadecylketene molecular ion with $m/z$ 55 (the most intense ion in the MS spectra of ketenes) and 42, 56, 70, 84, 98, 112, and 126 obtained during decomposition of the chemically bonded stearic acid fragment.

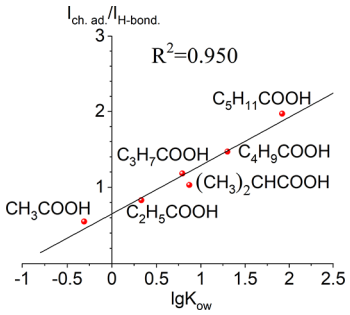


**Figure 11.** Correlation between the carboxylic acids' hydrophobic properties (as defined by the *n*-octanol/water partition coefficient lg$K_{ow}$) and the intensity ratio $I_{ch.\ ad.}/I_{H\text{-}bond.}$

formation of complexes, which is directly related to the hydrophobicity of the system. Probably, it could be associated with complexes formation with the parallel orientation to the surface like on Scheme 1, surface complexes SC IIIa and SC IIIb, because, in this case, the hydrophobicity has a significant impact on the complex stability and, as a result, on their preferable formation on the surface.

The ratio of TPD-peak intensities (decomposition of adsorpted complex to destruction of hydrogen-bonded complex) is linked with the substrate's hydrophobicity parameter, lg$K_{ow}$, a quantitative measure of the compound's distribution between aqueous and organic phases from literature data (Table 4). Values of lg$K_{ow}$ can be calculated using an additive (atom and group contributions) method, i.e., a molecule is dissected into primary fragments (functional groups or atoms) in which lg$K_{ow}$ is known.[60] Basically, the higher the compound's hydrophobicity, the more positive value of lg$K_{ow}$ is.[60,61] Calculations of lg$K_{ow}$ values for 2-methylpropanoic and 2,2-dimethylpropanoic acids were carried out using Hansch and Leo's compilation (additive method).[60] Indeed, an excellent correlation is observed between the $I_{ch.ad.}/I_{H\text{-bond}}$ ratio and the hydrophobicity parameter lg$K_{ow}$ (Figure 11, Table 4).[60]

*3.4.1. Evaluation of Quantity of Each Complex.* The percentage of each acid form on the silica surface in Scheme 1 can be calculated by using deconvoluted TPD data. The area under each peak in the TPD curve is proportional to the amount of the corresponding adsorption mode (Table 5). It can be calculated considering the area of each peak as a proportion of the total TPD area as the total amount of acid adsorbed (Table 5).

The measurement of areas in the TPD of silica-supported ethanoic acid is illustrated in Figure S3 (Supporting Information). Similarly, the calculations of adsorbed butanoic (Figure 12) and octadecanoic acids (Figure S4 (Supporting Information)) have been conducted for the curve at $m/z$ 55, i.e., the most intense on ketenes' thermal desorption curves. There is no peak of hydrogen-bonded acid on TPD-curves of octadecanoic acid, the longest length of the aliphatic chain considered (Figure S4 (Supporting Information)), meaning that the TPD peaks are formed by dimers (complex I) and adsorbed acids.

The semiquantitative data based on TPD areas from the thermolysis of ethanoic, butanoic, and octadecanoic acids are represented in Table 5. It shows that the amount of adsorbed ethanoic and butanoic acids is practically the same, even though the aliphatic chain differs only by two $CH_2$ groups. A significant variation is found between ethanoic and octadecanoic acids, which have a chain length difference of 16 $CH_2$ groups. In a homologous series of carboxylic acids, the amount of acid chemisorbed on the silica surface increases with increasing hydrocarbon chain length; the total amount of chemisorbed acids is formed by 70% octadecanoic acid, 13% butanoic acid, and 14% ethanoic acid.

**3.5. Pyrolysis of Triglycerides and Waste Biomass, Rapeseed Meal.** In order to confirm that results for fatty acids could be extended for waste biomass (and can be applied to 2G biomass conversion processes), additional studies of the

**Table 4. Physico-Chemical Parameters of Aliphatic Carboxylic Acids and Ratio of Peak Intensities (Decomposition of Adsorpted Complex to Destruction of Hydrogen-bonded Complex)**

| acid | chemical formula | $T_b$, °C | p$K_a$[59] | lg$K_{ow}$ | $I_{ch.\ ad}/I_{H\text{-bond}}$ |
|---|---|---|---|---|---|
| methanoic | HCOOH | 100.7 | 3.75 | −0.54 | - |
| ethanoic | $CH_3COOH$ | 117.72 | 4.756 | −0.31 | 0.55 I($m/z$ 42)/I($m/z$ 60) |
| propanoic | $CH_3CH_2COOH$ | 140.8 | 4.87 | 0.33; 0.25 | 0.83 I($m/z$ 56)/I($m/z$ 74) |
| butanoic | $CH_3(CH_2)_2COOH$ | 163.25 | 4.83 | 0.79 | 1.18 I($m/z$ 55)/I($m/z$ 60) |
| 2-methylpropanoic | $(CH_3)_2CHCOOH$ | | 4.84 | 0.87 calculated according to additive method[60] | 1.03 I($m/z$ 55)/I($m/z$ 60) |
| pentanoic | $CH_3(CH_2)_3COOH$ | 186.35 | 4.83 | 1.30 ($Et_2O$) | 1.47 I($m/z$ 55)/I($m/z$ 60) |
| hexanoic | $CH_3(CH_2)_4COOH$ | 205.35 | 4.85 | 1.92 | 1.97 I($m/z$ 55)/I($m/z$ 60) |
| 2.2-dimethylpropanoic | $(CH_3)_3CCOOH$ | | 5.03 | 1.31 calculated according to additive method[60] | ∞ |
| octadecanoic acid(stearic) | $C_{17}H_{35}COOH$ | 376.1 | 4.5[61] | 8.23 (estimated)[61] | ∞ |


https://doi.org/10.1021/jacs.3c06966
J. Am. Chem. Soc. XXXX, XXX, XXX−XXX

**Table 5. Calculation of the Relative Amount (fraction) of Surface Complexes I (Scheme 1A), II (Scheme 1B), III (Scheme 1C), and IV (Scheme 1D) According to TPD-MS Data[a]**

| acid, triglyceride, biomass | surface complex | $T_{max}$, °C | $m/z$ | $\int(I(m/z))$ | % | $A_{surf}$, mmol·g$^{-1}$ | $n$ | $E^{\#}$, kJ · mol$^{-1}$ | $k_0$, s$^{-1}$ | $\Delta S^{\#}$, cal·K$^{-1}$ · mol$^{-1}$ | $R^2$ |
|---|---|---|---|---|---|---|---|---|---|---|---|
| Fatty Acids | | | | | | | | | | | |
| ethanoic (0.3 mmol·g$^{-1}$) | I | 72 | 60 | 330 | 49 | 0.147 | 1 | 72* | | | |
| | II | 127 | 60 | 250 | 37 | 0.111 | 1 | 83* | | | |
| | III/IV | 326 | 42 | 93 | 14 | 0.042 | 1 | 104 | $4.27 \times 10^6$ | −30 | 0.924 |
| butanoic (0.4 mmol·g$^{-1}$) | I | 85 | 60 | 53 | 48 | 0.192 | 1 | 75* | | | |
| | II | 154 | 60 | 38 | 35 | 0.14 | 1 | 89* | | | |
| | III/IV | 354 | 55 | 14 | 13 | 0.052 | 1 | 104 | $1.55 \times 10^6$ | −31 | 0.930 |
| octadecanoic (0.6 mmol·g$^{-1}$) | I | 62 | 60 | 38 | 30 | 0.18 | 1 | 70* | | | |
| | II | | | | | | | | | | |
| | III/IV | 380 | 55 | 89 | 70 | 0.42 | 1 | 113 | $5.04 \times 10^6$ | −30 | 0.977 |
| | | 377 | 70 | | | | 1 | 113 | $4.49 \times 10^6$ | −30 | 0.940 |
| | | 378 | 84 | | | | 1 | 115 | $7.21 \times 10^6$ | −29 | 0.956 |
| | | 383 | 98 | | | | 1 | 115 | $7.20 \times 10^6$ | −29 | 0.976 |
| | | 381 | 112 | | | | 1 | 116 | $7.07 \times 10^6$ | −29 | 0.914 |
| Triglyceride | | | | | | | | | | | |
| glyceryl trimyristate | | 358 | 126 | | | | 1 | 110 | $6.16 \times 10^6$ | −29 | 0.960 |
| | | 354 | 112 | | | | 1 | 111 | $6.99 \times 10^6$ | −29 | 0.941 |
| | | 354 | 98 | | | | 1 | 111 | $7.77 \times 10^6$ | −28 | 0.985 |
| | | 354 | 84 | | | | 1 | 111 | $8.73 \times 10^6$ | −28 | 0.989 |
| | | 358 | 70 | | | | 1 | 110 | $6.60 \times 10^6$ | −29 | 0.990 |
| | | 351 | 55 | | | | 1 | 109 | $4.32 \times 10^6$ | −30 | 0.957 |
| Waste Oil Crop Biomass | | | | | | | | | | | |
| rapeseed meal | | ~360 | 112 | | | | | | | | |
| | | 367 | 98 | | | | 1 | 113 | $5.30 \times 10^6$ | −29 | 0.930 |
| | | 362 | 84 | | | | 1 | 110 | $3.24 \times 10^6$ | −30 | 0.957 |
| | | 362 | 70 | | | | 1 | 113 | $5.72 \times 10^6$ | −29 | 0.911 |
| | | 367 | 55 | | | | 1 | 114 | $5.14 \times 10^6$ | −29 | 0.944 |

[a]Kinetic parameters (temperature of maximum reaction rate $T_{max}$, reaction order $n$, activation energy $E^{\neq}$, pre-exponential factor $k_0$, change of activation entropy $\Delta S^{\neq}$) obtained during the pyrolysis of fatty acids, glyceryl trimyristate, and rapeseed meal over silica. *, Calculated approximately from equation $E^{\#} = 25RT_{max}$.

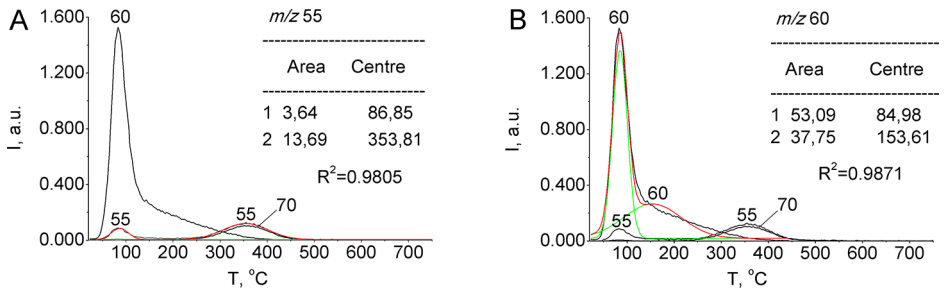


**Figure 12.** Curve-fitting of deconvoluted TPD-traces of the silica-supported butanoic (butyric) acid sample (0.4 mmol·g$^{-1}$) for ions at $m/z$ 55 (A) and $m/z$ 60 (B).

pyrolysis kinetics of trimyristin and rapeseed meal over silica were subsequently conducted.

A set of ions characteristic of ketene myristic acid, dodecyl ketene, is observed in the mass spectra of volatile pyrolysis products of glycerol myristic (tetradecanoic) acid over silica at temperatures above 250°C (Figure 13A,B). The most intense ion in the mass spectra of ketenes is $[H_2C{=}C{=}C{=}O{-}H]^+$ with $m/z$ 55 and a set of ions with the general formula $[H(CH_2)_n{-}(H)C{=}C{=}O]^+$, which was observed for ketenes synthesized by catalytic pyrolysis from the homologous series of C1···C10 acids.[19,57] In the case of trimyristin, a set of ions with $n$ = 0···10 is observed: $m/z$ 42, 56, 70, 84, 98, 112, 126, 140, etc., Figure13A,B. At the same time, as the mass of the ion increases, its intensity decreases significantly, especially after $m/z$ 98, and the molecular ion for long-chain ketenes, as a rule, is not observed, for example, for octyl ketene during pyrolysis of decanoic acid.[19,57,63] A peak is observed at $T_{max} \approx 350$°C on the TPD curves for these ions. That is, the temperature of the maximum desorption rate and, accordingly, the activation energy of dodecylketene formation ($T_{max}$ = 355°C, $E^{\neq}_{average}$ = 110 kJ·mol$^{-1}$) is lower than that of hexadecylketene ($T_{max}$ = 380°C, $E^{\neq}_{average}$ = 114.4 kJ·mol$^{-1}$) in the case of pyrolysis of octadecanoic (stearic) acid (Figure 10, Table 5). This probably indicates that ketene formation occurs due to the transformation of the surface complex of free myristic acid, which is not connected by an ester bond with glycerol (silica is known to effectively hydrolyze ester bonds).


https://doi.org/10.1021/jacs.3c06966
J. Am. Chem. Soc. XXXX, XXX, XXX−XXX

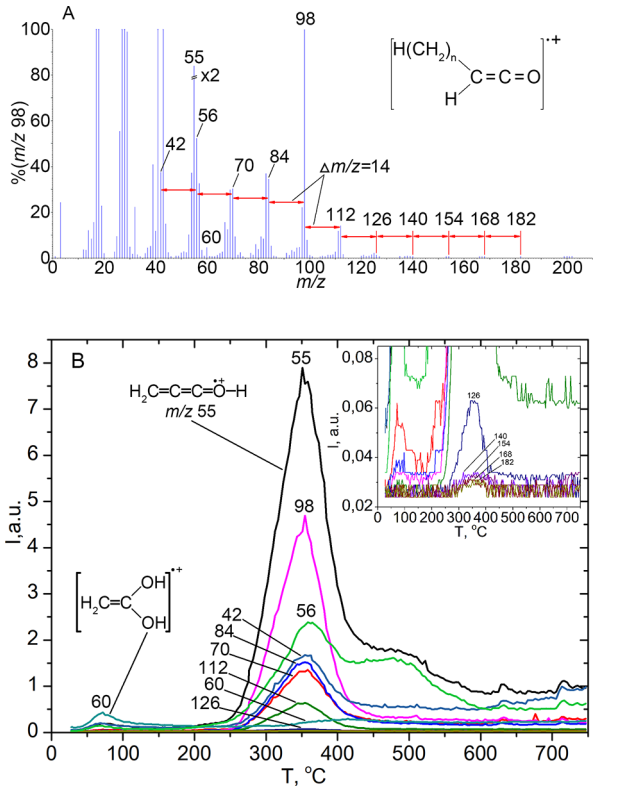


**Figure 13.** (A) Mass spectra of volatile pyrolysis products at a temperature of 350°C and (B) TPD-curves obtained during pyrolysis of glyceryl trimyristate over silica.

The hydrolysis of dicarboxylic esters, including long-chained aliphatic carboxylic acids with high selectivity and yield at temperatures ~220°C, was carried out by Dyker.[64] Undoubtedly, trimyristin is also hydrolyzed on the surface of silica when heated to ~200°C. As we can see (Figure 13B), low intensity peaks on the TPD curves for ions characteristic of free fatty acids, especially for the most intense ion $[H_2C{=}C(OH)_2]^+$ with $m/z$ 60[65] at a temperature around 100°C, are observed. That indicates the absence of physisorbed and H-bonded forms of the acid (surface complexes I and II, Scheme 1), which were observed for the short-chain and long-chain acids, such as octadecanoic (stearic) (Figures 10 and 12, Table 5). So, hydrolysis mainly occurs during heating, which is absent when triglyceride is loaded on the silica surface. Therefore, triglyceride hydrolysis occurs during heating, forming a surface complex of myristic acid, which is then subjected to ketenization (Scheme 2).

Some publications report on the processes of formation of short-chain fatty acids and some unsaturated aromatic and polyaromatic hydrocarbon due to C−C bond cleavage during fast pyrolysis and thermal cracking of triglycerides.[66] However, higher pyrolysis temperatures (750 (30 s) and 450 °C (30 s)), higher heating rates of 800°C/min, cracking at high pressures up to 37 MPa, or various catalysts had to be employed.[66] In our case of pyrolysis on the silica surface, the main process is ketenization. We can monitor if the cracking of triglycerides with C−C bond cleavage and the formation of short-chain acids are evolving by the TPD curve of the most intense characteristic ion with $m/z$ 60 in the mass spectra of carboxylic acids. From the analysis of the behavior of the TPD curve with $m/z$ 60, these processes (if taking place at all) occur at higher temperatures (>400°C). Their contribution to the overall pyrolysis process is minimum since the intensity of the ion $m/z$ 60 contributes with a small percentage as compared to the intensity of the ion with $m/z$ 55, Figure 13B.

Silica allowed us to avoid the additional stage of hydrolysis of esters in converting 2G biomass rich in triglycerides and lipids. This has a significant economic benefit to develop waste oil crop biomass pyrolysis technologies—especially biomass from rapeseed crops and soybeans, the two largest oil crops grown worldwide.[67] Rapeseed production reached 29 million

**Scheme 2. Possible Mechanism of Triglyceride Hydrolysis over Silica with Forming a Surface Complex of Myristic Acid, Which Is Then Subjected to the Ketenization Reaction; EI Fragmentation of Molecular Ion of Dodecylketene and Structures of Its Fragment Ions**

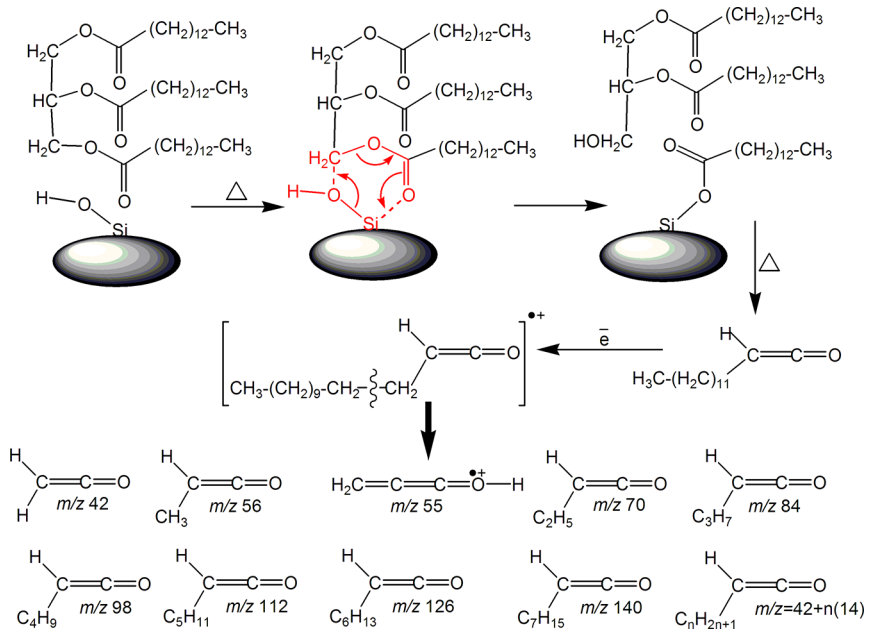




https://doi.org/10.1021/jacs.3c06966
J. Am. Chem. Soc. XXXX, XXX, XXX−XXX

tons in 2022. At the same time, the annual production of waste oil crop meal reached 71 million tons.[68] The rapeseed meal is the primary waste produced via oil pressing. Accordingly, this byproduct has a high triglyceride content. However, this type of biomass is different from lignocellulosic biomass, and therefore, for its effective processing, it requires establishing the patterns of pyrolysis of the main components, particularly fatty acids and triglycerides. The lipid content in rapeseed meals reaches 7−10%, while rapeseed seeds contain a high amount of mono- and polyunsaturated fatty acids (around 90%) and low concentrations (6.5−8%) of saturated fatty acids.[69,70]

The kinetics of pyrolysis of canola meal depend mainly on its fatty acid composition, comprising ca. 60% (*Z*)-octadec-9-enoic acid (oleic acid) (C18:1), 10% (9*Z*,12*Z*,15*Z*)-octadeca-9,12,15-trienoic acid (linolenic acid) (C18:3), 24% (9*Z*,12*Z*)-octadeca-9,12-dienoic acid (linoleic acid) (C18:3), 4% hexadecanoic acid (palmitic acid) (C16:0), 2% octadecanoic acid (stearic acid) (C18:0), 0.25% tetradecanoic acid (myristic acid) (C14:0), and others.[69] Since almost 95% of the oil consists of acids with a chain length of C18, they will determine the kinetics of canola meal pyrolysis. As can be seen, the temperature of the maximum desorption rate of octadecylketene during pyrolysis of octadecanoic acid (stearic acid) at C18 is about 380 °C, Figure 10, Table 5. That is, this temperature is slightly higher with respect to 370 °C (localization of peaks on TPD curves of the characteristic ions of ketenes with *m*/*z* 55, 70, 84, 98, and 112 during the pyrolysis of rapeseed cake, Figure 14, Table 5). This is quite

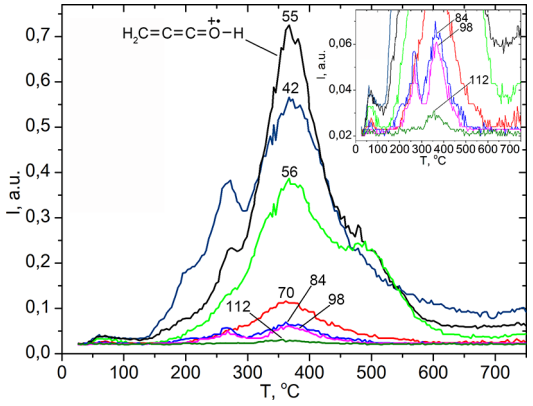


**Figure 14.** TPD-curves of ketene fragment ions with *m*/*z* 42, 55, 56, 70, 84, 98, and 112 obtained during pyrolysis of rapeseed meal over silica.

natural since C16:0 palmitic acid, which in rapeseed oil reaches 6%, also contributes to the formation of these peaks on the TPD curves of ketene fragment ions and, as a result, shifts them to a lower temperature. Our previous work[19] showed that the temperature of the maximum rate of ketene desorption increases with an increase in the length of the hydrocarbon chain of the acid. Accordingly, the activation energy of the ketenization reaction on the silica surface increases, Figure 15, Table 5. This is precisely why an increase in activation energy is observed in the following order: trimyristat ($E^{\neq}_{average}$ = 110 kJ·mol$^{-1}$) < rapeseed meal ($E^{\neq}_{average}$ = 112.5 kJ·mol$^{-1}$) < stearic acid ($E^{\neq}_{average}$ = 114.4 kJ·mol$^{-1}$), Table 5.

In addition, a "structure−reactivity" correlation was found between $E^{\neq}$ and Taft induction constants of substituents ($E^{\neq}$ = 109.6 − 13.457 $\Sigma\sigma^*$) for the ketenization reaction. On the

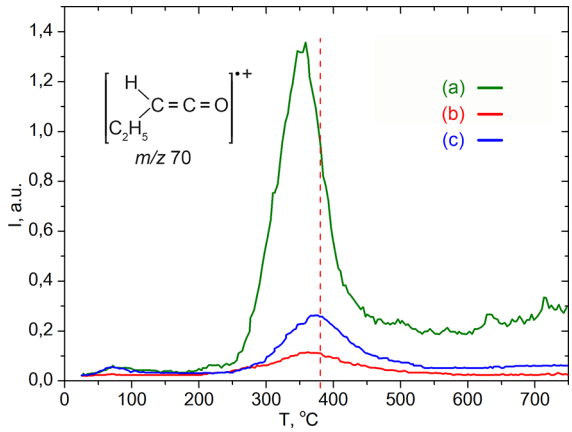


**Figure 15.** TPD-curves of ketenes fragment ions with *m*/*z* 70 obtained during pyrolysis of (a) glyceryl trimyristate, (b) stearic acid and, and (c) rapeseed meal (*Camelina sativa*) over silica.

other hand, in the case of the ketonization reaction over ceria for a homologous series of acids, a correlation between the activation energy and the Taft steric constants of the substituents ($E^{\neq}$ = 126,84 − 3.096 $\Sigma$Es*) was revealed.[14] $T_{max}$ is the most sensitive characteristic of the effect of substituents on reaction kinetics. In addition, $T_{max}$ reproduced in TPD experiments very accurately; because of this, many approximate equations using $T_{max}$ were proposed to calculate approximate values of the activation energy,[19,39,71] the reaction parameter $p_o$,[19] and the kinetic isotope effect.[3,14]

In the spectra of volatile products of rapeseed meal pyrolysis over silica, there are no ions larger than *m*/*z* 112 (Figure 14). This is related to the features of fragmentation and ion-molecular reactions of molecular ions of ketenes of unsaturated acids (C18:1, C18:2, and C18:3) under the action of electron impact in the ion source of the mass spectrometer. This feature is due to their structure, particularly double bonds in their molecules, Scheme 3. It is known[72] that the primary way of alkenes fragmentation under electron impact is C−C bond cleavage in the beta position to the double bond, with the formation of allylic fragments, stabilized due to resonance (Scheme 3). In the case of molecular ions of ketenes of unsaturated acids, the predominant channel of transformation of the molecular ion will be C7−C6 bond cleavage with the formation of fragment ion *m*/*z* 112 (Scheme 3). The patterns obtained for fatty acids, triglycerides, and rapeseed meal in this work are of practical importance and can be used in the future in the development of sustainable technologies for the conversion of 2G biomass with a high content of triglycerides in the processing of oils/fats production waste and related waste feedstocks.

**3.6. Thermogravimetric Analysis.** Thermogravimetric analyses of silica and silica-supported acids were performed by soaking them in $CCl_4$ solutions. The peaks at $T_{max}$ = 62 and 100−200°C and a broader peak at the temperature range of 200−500°C were observed on the derivative thermogravimetry (DTG) curve (Figure 16). The first peak is associated with desorption from the silica surface of the physically adsorbed solvent ($CCl_4$) or carboxylic acid dimers. The second one in the temperature region $T_{max}$ = 100−200°C would be associated with the decomposition of the hydrogen-bonded acid on the silica surface. The third and fourth peaks are related to the desorption of products from the dehydration and


https://doi.org/10.1021/jacs.3c06966
J. Am. Chem. Soc. XXXX, XXX, XXX−XXX

**Scheme 3. Thermal Decomposition of Triglycerides of Unsaturated Fatty Acids (Oleic, Linoleic, and Linolenic Acids) from Rapeseed Meal; Structure of Fragment Ions of Ketenes Obtained via EI Ionization**

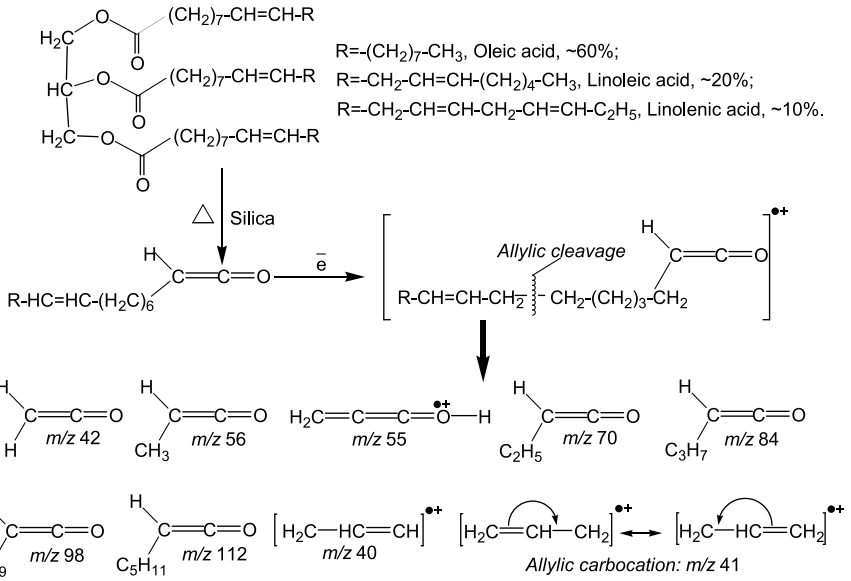


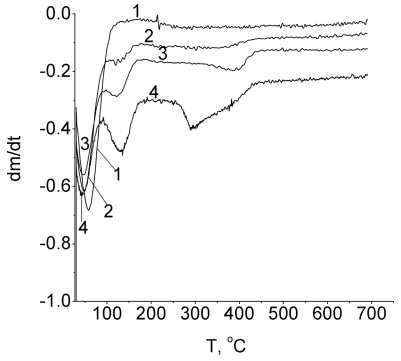


**Figure 16.** DTG curves of silica (line 1) and silica-supported samples of acids: propanoic (line 2), 2-methylpropanoic acid (line 3), and pentanoic (line 4).

dehydroxylation processes, which take place in the temperate region 200−500°C.

On previous TPD results,[19] the peak for complex II, $T_{max}$, appears in the temperature region 120−150°C (ethanoic − $T_{max}$ = 127°C; butanoic − $T_{max}$ = 154 °C) and practically coincides with the peak attributed to complex II on DTG curves. In the same way, the decomposition of complexes III/IV on TPD curves in the temperature range 360−390 °C[62] agrees with the DTG peak (~390°C) regarding the decomposition of complex IV. Therefore, TPD and DTG indicate a few decomposition stages of adsorbed compounds. In contrast, the differences between these techniques are attributed to the presence of oxygen during DTG thermal decomposition.

## 4. CONCLUSIONS

The interaction of linear and branched aliphatic carboxylic acids C1−C6, C18, triglyceride, and rapeseed meal with the fumed silica surface has been studied. Isotherms and physicochemical parameters of short fatty acid C1−C6 adsorption from an aqueous medium were obtained. The formation of different adsorption modes was identified using *in situ* IR spectroscopy, FTIR, thermogravimetry, TPD-MS, and DFT calculations. The observed adsorption modes are dimers bonded with the surface via van der Waals, hydrogen-bonded complexes, and adsorbed complexes bonded on the surface via the C═O group; their relative abundance and decomposition activation energies were obtained. A correlation between the hydrophobicity parameter $lgK_{o/w}$ and TPD intensities ratio of peaks assigned to decomposing hydrogen-bonded and C═O bonded complexes for studied acids has been obtained. These results indicate the significant contribution of hydrophobic interactions to the binding of fatty acids with silica. Notably, the formation of surface complexes coordinating the carboxyl oxygen and the silicon atom of the surface leads to a penta-coordinated Si atom, as confirmed by DFT simulations using both "soft" and "hard" model of the silica surface. Moreover, it was strongly confirmed on expanded "hard" model calculations through significantly decreasing the bond length between the Si atom and the O atom of acid. Besides fatty acids, two types of surface water were observed in the IR-spectra ($\delta_{(H-O-H)}$ at ~1640 and ~1615 $cm^{-1}$), which remained on the surface until all chemisorbed acids were converted into ketenes, indicating the bonding of acids with strained siloxane bridges. Most importantly, these insightful studies support the fact that the established features observed from the ketene formation reaction can also be in principle extended to higher aliphatic acids, triglycerides, and waste biomass. These can pave the way to the design of environmentally safe technologies to process renewable biomass, plant triglycerides, and waste feedstocks into high-value-added products, including fine chemicals and fuels.

## ■ ASSOCIATED CONTENT

### Supporting Information

The Supporting Information is available free of charge at https://pubs.acs.org/doi/10.1021/jacs.3c06966.

IR spectra of propanoic and hexanoic acids impregnated on the silica surface with different loadings (0.15−0.6 mmol·$g^{-1}$) and the curve-fitted data from deconvoluted TPD-traces for ethanoic and octadecanoic acids supported on silica (PDF)



https://doi.org/10.1021/jacs.3c06966
J. Am. Chem. Soc. XXXX, XXX, XXX−XXX

## AUTHOR INFORMATION


### Corresponding Authors

**Liana R. Azizova** − *School of Dentistry, Cardiff University, Cardiff CF14 4XY, U.K.; Chuiko Institute of Surface Chemistry, National Academy of Science of Ukraine, Kyiv 03164, Ukraine;* orcid.org/0000-0001-7096-4452; Email: AzizovaL@cardiff.ac.uk

**Tetiana V. Kulik** − *Chuiko Institute of Surface Chemistry, National Academy of Science of Ukraine, Kyiv 03164, Ukraine; Cardiff Catalysis Institute, School of Chemistry, Cardiff University, Cardiff CF10 3AT, U.K.;* orcid.org/0000-0002-1740-0348; Email: KulykT@cardiff.ac.uk

### Authors

**Borys B. Palianytsia** − *Chuiko Institute of Surface Chemistry, National Academy of Science of Ukraine, Kyiv 03164, Ukraine; Departamento de Química Orgánica, Universidad de Córdoba, Cordoba E14014, Spain;* orcid.org/0000-0002-6676-632X

**Mykola M. Ilchenko** − *Institute of Molecular Biology and Genetics, National Academy of Science of Ukraine, Kyiv 03680, Ukraine*

**German M. Telbiz** − *National Academy of Science of Ukraine, L. V. Pisarzhevsky Institute of Physical Chemistry, Kyiv 03039, Ukraine*

**Alina M. Balu** − *Departamento de Química Orgánica, Universidad de Córdoba, Cordoba E14014, Spain*

**Sergiy Tarnavskiy** − *Institute of Molecular Biology and Genetics, National Academy of Science of Ukraine, Kyiv 03680, Ukraine*

**Rafael Luque** − *Universitá degli studi Mediterranea di Reggio Calabria (UNIRC), DICEAM, Via Zehender (giá via Graziella), I89122 Reggio Calabria, Italy; Universidad ECOTEC, Samborondón EC092302, Ecuador;* orcid.org/0000-0003-4190-1916

**Alberto Roldan** − *Cardiff Catalysis Institute, School of Chemistry, Cardiff University, Cardiff CF10 3AT, U.K.;* orcid.org/0000-0003-0353-9004

**Mykola T. Kartel** − *Chuiko Institute of Surface Chemistry, National Academy of Science of Ukraine, Kyiv 03164, Ukraine*

Complete contact information is available at: https://pubs.acs.org/10.1021/jacs.3c06966

### Author Contributions

◆This coauthor has passed away. Date of death: September 21, 2021. The manuscript was written through contributions of all authors.


### Notes

The authors declare no competing financial interest.

## ACKNOWLEDGMENTS

T.K. acknowledges the British Academy's Researchers at Risk Fellowships Programme for partially supporting this research. This work was partially supported by Project 101057430 SusPharma (HORIZON-HLTH-2021-IND-07) and by the grant FSA3-20-66700 from the U.S. Civilian Research & Development Foundation (CRDF Global) with funding from the United States Department of State. B.P. thanks Ministerio de Ciencia e Innovación, Gobierno de España (Project MCIN/AEI/10) for partially supporting this work. This work was performed using computational facilities of the joint computer cluster of SSI "Institute for Single Crystals" of the National Academy of Sciences of Ukraine and the Institute for Scintillation Materials of the National Academy of Sciences of Ukraine incorporated into the Ukrainian National Grid. R. Luque gratefully acknowledges support from DICEAM and Universitá degli studi Mediterranea di Reggio Calabria (UNIRC) for the provision of the Rosario Pietropaolo Honorary Chair. We would also like to thank the Armed Forces of Ukraine for providing security to perform this work.

## REFERENCES

(1) Orjuela, A.; Clark, J. Green chemicals from used cooking oils: Trends, challenges, and opportunities. *Current Opinion in Green and Sustainable Chemistry* **2020**, *26*, No. 100369.

(2) Lestari, S.; Mäki-Arvela, P.; Beltramini, J.; Lu, G. Q. M.; Murzin, D. Y. Transforming Triglycerides and Fatty Acids into Biofuels. *ChemSusChem* **2009**, *2* (12), 1109−1119.

(3) Len, T.; Bressi, V.; Balu, A. M.; Kulik, T.; Korchuganova, O.; Palianytsia, B.; Espro, C.; Luque, R. Thermokinetics of production of biochar from crop residues: an overview. *Green Chem.* **2022**, *24* (20), 7801−7817.

(4) Lappi, H.; Alén, R. Production of vegetable oil-based biofuels—Thermochemical behavior of fatty acid sodium salts during pyrolysis. *Journal of Analytical and Applied Pyrolysis* **2009**, *86* (2), 274−280. Zhenyi, C.; Xing, J. I.; Shuyuan, L. I.; Li, L. I. Thermodynamics Calculation of the Pyrolysis of Vegetable Oils. *Energy Sources* **2004**, *26* (9), 849−856.

(5) Chiaramonti, D.; Buffi, M.; Rizzo, A. M.; Lotti, G.; Prussi, M. Bio-hydrocarbons through catalytic pyrolysis of used cooking oils and fatty acids for sustainable jet and road fuel production. *Biomass and Bioenergy* **2016**, *95*, 424−435.

(6) Calvo-Flores, F. G.; Martin-Martinez, F. J. Biorefineries: Achievements and challenges for a bio-based economy. *Front. Chem.* **2022**, *10*, No. 973417, DOI: 10.3389/fchem.2022.973417.

(7) (a) Kumar, A.; Shende, D. Z.; Wasewar, K. L. Production of levulinic acid: A promising building block material for pharmaceutical and food industry. *Materials Today: Proceedings* **2020**, *29*, 790−793. (b) Rose, P. K. Bioconversion of Agricultural Residue into Biofuel and High-Value Biochemicals: Recent Advancement. In *Zero Waste Biorefinery*, Nandabalan, Y. K., Garg, V. K., Labhsetwar, N. K., Singh, A., Eds.; Springer Nature Singapore, 2022; pp 233−268. (c) Lange, J.-P.; Price, R.; Ayoub, P. M.; Louis, J.; Petrus, L.; Clarke, L.; Gosselink, H. Valeric Biofuels: A Platform of Cellulosic Transportation Fuels. *Angew. Chem., Int. Ed.* **2010**, *49* (26), 4479−4483. (d) Serrano-Ruiz, J. C.; Braden, D. J.; West, R. M.; Dumesic, J. A. Conversion of cellulose to hydrocarbon fuels by progressive removal of oxygen. *Applied Catalysis B: Environmental* **2010**, *100* (1), 184−189.

(8) Biermann, U.; Bornscheuer, U. T.; Feussner, I.; Meier, M. A. R.; Metzger, J. O. Fatty Acids and their Derivatives as Renewable Platform Molecules for the Chemical Industry. *Angew. Chem., Int. Ed.* **2021**, *60* (37), 20144−20165. Becker, J.; Lange, A.; Fabarius, J.; Wittmann, C. Top value platform chemicals: bio-based production of organic acids. *Curr. Opin. Biotechnol.* **2015**, *36*, 168−175. Sudhakaran, S.; Taketoshi, A.; Siddiki, S. M. A. H.; Murayama, T.; Nomura, K. Transesterification of Ethyl-10-undecenoate Using a Cu-Deposited $V_2O_5$ Catalyst as a Model Reaction for Efficient Conversion of Plant Oils to Monomers and Fine Chemicals. *ACS Omega* **2022**, *7* (5), 4372−4380. He, S.; Klein, F. G. H.; Kramer, T. S.; Chandel, A.; Tegudeer, Z.; Heeres, A.; Heeres, H. J. Catalytic Conversion of Free Fatty Acids to Bio-Based Aromatics: A Model Investigation Using Oleic Acid and an H-ZSM-5/$Al_2O_3$ Catalyst. *ACS Sustainable Chem. Eng.* **2021**, *9* (3), 1128−1141. Gandini, A. The irruption of polymers from renewable resources on the scene of macromolecular science and technology. *Green Chem.* **2011**, *13* (5), 1061−1083.

(9) Araújo, A. M. d. M.; Lima, R. d. O.; Gondim, A. D.; Diniz, J.; Souza, L. D.; Araujo, A. S. d. Thermal and catalytic pyrolysis of

sunflower oil using AlMCM-41. *Renewable Energy* **2017**, *101*, 900−906.
(10) Sani, Y. M.; Daud, W. M. A. W.; Abdul Aziz, A. R. Activity of solid acid catalysts for biodiesel production: A critical review. *Applied Catalysis A: General* **2014**, *470*, 140−161. Salaheldeen, M.; Mariod, A. A.; Aroua, M. K.; Rahman, S. M. A.; Soudagar, M. E. M.; Fattah, I. M. R. Current State and Perspectives on Transesterification of Triglycerides for Biodiesel Production. *Catalysts* **2021**, *11* (9), 1121. Thangaraj, B.; Solomon, P. R.; Muniyandi, B.; Ranganathan, S.; Lin, L. Catalysis in biodiesel production—a review. *Clean Energy* **2019**, *3* (1), 2−23.
(11) Albrecht, K. O.; Olarte, M. V.; Wang, H. Upgrading Fast Pyrolysis Liquids. In *Thermochemical Processing of Biomass*, 2019; pp 207−255. Boekaerts, B.; Lorenz, W.; Van Aelst, J.; Sels, B. F. Kinetics of fatty acid ketonization in liquid phase with anatase and rutile $TiO_2$ catalysts. *Applied Catalysis B: Environmental* **2022**, *305*, No. 121052.
(12) Mansir, N.; Mohd Sidek, H.; Teo, S. H.; Mijan, N.-A.; Ghassan Alsultan, A.; Ng, C. H.; Shamsuddin, M. R.; Taufiq-Yap, Y. H. Catalytically active metal oxides studies for the conversion technology of carboxylic acids and bioresource based fatty acids to ketones: A review. *Bioresource Technology Reports* **2022**, *17*, No. 100988.
(13) Wang, F.; Yu, F.; Wei, Y.; Li, A.; Xu, S.; Lu, X. Promoting hydrocarbon production from fatty acid pyrolysis using transition metal or phosphorus modified Al-MCM-41 catalyst. *Journal of Analytical and Applied Pyrolysis* **2021**, *156*, No. 105146. Dyachenko, A.; Ischenko, O.; Diyuk, V.; Goncharuk, O.; Borysenko, M.; Mischanchuk, O.; Zakharova, T.; Pryhunova, O.; Sternik, D.; Lisnyak, V. The catalytic efficiency of Fe-containing nanocomposites based on highly dispersed silica in the reaction of $CO_2$ hydrogenation. *Res. Chem. Intermed.* **2022**, *48* (6), 2607−2625. Ischenko, O. V.; Dyachenko, A. G.; Saldan, I.; Lisnyak, V. V.; Diyuk, V. E.; Vakaliuk, A. V.; Yatsymyrskyi, A. V.; Gaidai, S. V.; Zakharova, T. M.; Makota, O.; et al. Methanation of CO2 on bulk Co−Fe catalysts. *Int. J. Hydrogen Energy* **2021**, *46* (76), 37860−37871. Dyachenko, A. G.; Ischenko, O. V.; Goncharuk, O. V.; Borysenko, M. V.; Mischanchuk, O. V.; Gun'ko, V. M.; Sternik, D.; Lisnyak, V. V. Preparation and characterization of Ni−Co/$SiO_2$ nanocomposite catalysts for $CO_2$ methanation. *Applied. Nanoscience* **2022**, *12* (3), 349−359. Guntida, A.; Rattanachartnarong, T.; Jongsomjit, B.; Sooknoi, T.; Weerachawanasak, P.; Praserthdam, S.; Praserthdam, P. Determining the role of oxygen vacancies in palmitone selectivity and coke formation over acid metal oxide catalysts for the ketonization of methyl palmitate. *Applied Catalysis A: General* **2021**, *628*, No. 118405. Boekaerts, B.; Sels, B. F. Catalytic advancements in carboxylic acid ketonization and its perspectives on biomass valorisation. *Applied Catalysis B: Environmental* **2021**, *283*, No. 119607. Fufachev, E. V.; Weckhuysen, B. M.; Bruijnincx, P. C. A. Toward Catalytic Ketonization of Volatile Fatty Acids Extracted from Fermented Wastewater by Adsorption. *ACS Sustainable Chem. Eng.* **2020**, *8* (30), 11292−11298.
(14) Kulik, T.; Palianytsia, B.; Larsson, M. Catalytic Pyrolysis of Aliphatic Carboxylic Acids into Symmetric Ketones over Ceria-Based Catalysts: Kinetics, Isotope Effect and Mechanism. *Catalysts* **2020**, *10* (2), 179.
(15) Kulyk, K.; Palianytsia, B.; Alexander, J. D.; Azizova, L.; Borysenko, M.; Kartel, M.; Larsson, M.; Kulik, T. Kinetics of Valeric Acid Ketonization and Ketenization in Catalytic Pyrolysis on Nanosized $SiO_2$, $\gamma$-$Al_2O_3$, $CeO_2/SiO_2$, $Al_2O_3/SiO_2$ and $TiO_2/SiO_2$. *ChemPhysChem* **2017**, *18* (14), 1943−1955.
(16) Maree, D. C.; Heydenrych, M. Development of a Mesoporous Silica-Supported Layered Double Hydroxide Catalyst for the Reduction of Oxygenated Compounds in E. grandis Fast Pyrolysis Oils. *Catalysts* **2021**, *11* (12), 1527. Lombard, C. J.; van Sittert, C. G. C. E.; Mugo, J. N.; Perry, C.; Willock, D. J. Computational investigation of $\alpha$-$SiO_2$ surfaces as a support for Pd. *Phys. Chem. Chem. Phys.* **2023**, *25* (8), 6121−6130.
(17) Allen, A. D.; Tidwell, T. T. Ketenes and Other Cumulenes as Reactive Intermediates. *Chem. Rev.* **2013**, *113* (9), 7287−7342.
(18) Smallman, H. R.; Leitch, J. A.; McBride, T.; Ley, S. V.; Browne, D. L. Formation and utility of reactive ketene intermediates under continuous flow conditions. *Tetrahedron* **2021**, *93*, No. 132305.
(19) Kulik, T. V. Use of TPD−MS and Linear Free Energy Relationships for Assessing the Reactivity of Aliphatic Carboxylic Acids on a Silica Surface. *J. Phys. Chem. C* **2012**, *116* (1), 570−580.
(20) Tidwell, T. T. *Ketenes II*; John Wiley & Sons, 2006.
(21) Libby, M. C.; Watson, P. C.; Barteau, M. A. Synthesis of Ketenes with Oxide Catalysts. *Ind. Eng. Chem. Res.* **1994**, *33* (12), 2904−2912.
(22) R Miller, R.; Abaecherli, C.; Said, A.; Jackson, B. Ketenes. In *Ullmann's Encyclopedia of Industrial Chemistry*; Wiley-VCH, 2001; pp 171 − 185.
(23) Heravi, M. M.; Talaei, B. Chapter Four - Ketenes as Privileged Synthons in the Syntheses of Heterocyclic Compounds. Part 1: Three- and Four-Membered Heterocycles. In *Adv. Heterocycl. Chem.*, Katritzky, A. R., Ed.; Vol. *113*; Academic Press, 2014; pp 143−244. Heravi, M. M.; Talaei, B. Chapter Five - Ketenes as Privileged Synthons in the Synthesis of Heterocyclic Compounds Part 3: Six-Membered Heterocycles. In *Adv. Heterocycl. Chem.*, Scriven, E. F. V., Ramsden, C. A., Eds.; Vol. *118*; Academic Press, 2016; pp 195−291.
(24) Shelkov, R.; Nahmany, M.; Melman, A. Acylation through Ketene Intermediates. *Journal of Organic Chemistry* **2002**, *67* (25), 8975−8982. Badal, M. M. R.; Zhang, M.; Kobayashi, S.; Mishima, M. Amination of phenylketenes. Substituent effect on amine-catalyzed tautomerization of amide enol. *J. Phys. Org. Chem.* **2013**, *26* (12), 1071−1076. Sung, K.; Tidwell, T. T. Amination of Ketene: A Theoretical Study. *J. Am. Chem. Soc.* **1998**, *120* (13), 3043−3048.
(25) Resasco, D. E.; Wang, B.; Crossley, S. Zeolite-catalysed C−C bond forming reactions for biomass conversion to fuels and chemicals. *Catalysis Science & Technology* **2016**, *6* (8), 2543−2559.
(26) Bonati, M. L. M.; Joyner, R. W.; Stockenhuber, M. A temperature programmed desorption study of the interaction of acetic anhydride with zeolite beta (BEA). *Catal. Today* **2003**, *81* (4), 653−658.
(27) Fu, N.; Tidwell, T. T. Preparation of $\beta$-lactams by [2 + 2] cycloaddition of ketenes and imines. *Tetrahedron* **2008**, *64* (46), 10465−10496.
(28) Chowdhury, A. D.; Gascon, J. The Curious Case of Ketene in Zeolite Chemistry and Catalysis. *Angew. Chem., Int. Ed.* **2018**, *57* (46), 14982−14985. Gong, X.; Çağlayan, M.; Ye, Y.; Liu, K.; Gascon, J.; Dutta Chowdhury, A. First-Generation Organic Reaction Intermediates in Zeolite Chemistry and Catalysis. *Chem. Rev.* **2022**, *122* (18), 14275−14345. Hutchings, G. J.; Hunter, R.; Johnston, P.; Vanrensburg, L. J. Methanol Conversion to Hydrocarbons over Zeolite H-ZSM-5: Investigation of the Role of CO and Ketene in the Formation of the Initial C-C Bond. *J. Catal.* **1993**, *142* (2), 602−616.
(29) Gong, X.; Ye, Y.; Chowdhury, A. D. Evaluating the Role of Descriptor- and Spectator-Type Reaction Intermediates During the Early Phases of Zeolite Catalysis. *ACS Catal.* **2022**, *12* (24), 15463−15500.
(30) Zhang, Y.; Gao, P.; Jiao, F.; Chen, Y.; Ding, Y.; Hou, G.; Pan, X.; Bao, X. Chemistry of Ketene Transformation to Gasoline Catalyzed by H-SAPO-11. *J. Am. Chem. Soc.* **2022**, *144* (40), 18251−18258.
(31) Jiao, F.; Pan, X.; Gong, K.; Chen, Y.; Li, G.; Bao, X. Shape-Selective Zeolites Promote Ethylene Formation from Syngas via a Ketene Intermediate. *Angew. Chem., Int. Ed.* **2018**, *57* (17), 4692−4696.
(32) Pham, T. N.; Sooknoi, T.; Crossley, S. P.; Resasco, D. E. Ketonization of Carboxylic Acids: Mechanisms, Catalysts, and Implications for Biomass Conversion. *ACS Catal.* **2013**, *3* (11), 2456−2473.
(33) Chen, W.; Li, G.; Yi, X.; Day, S. J.; Tarach, K. A.; Liu, Z.; Liu, S.-B.; Edman Tsang, S. C.; Góra-Marek, K.; Zheng, A. Molecular Understanding of the Catalytic Consequence of Ketene Intermediates under Confinement. *J. Am. Chem. Soc.* **2021**, *143* (37), 15440−15452.
(34) Hemberger, P.; Pan, Z.; Bodi, A.; van Bokhoven, J. A.; Ormond, T. K.; Ellison, G. B.; Genossar, N.; Baraban, J. H. The Threshold


https://doi.org/10.1021/jacs.3c06966
J. Am. Chem. Soc. XXXX, XXX, XXX−XXX

Photoelectron Spectrum of Fulvenone: A Reactive Ketene Derivative in Lignin Valorization. *ChemPhysChem* **2020**, *21* (19), 2217−2222. Pan, Z.; Bodi, A.; van Bokhoven, J. A.; Hemberger, P. On the absolute photoionization cross section and threshold photoelectron spectrum of two reactive ketenes in lignin valorization: fulvenone and 2-carbonyl cyclohexadienone. *Phys. Chem. Chem. Phys.* **2022**, *24* (6), 3655−3663. Pan, Z.; Puente-Urbina, A.; Bodi, A.; van Bokhoven, J. A.; Hemberger, P. Isomer-dependent catalytic pyrolysis mechanism of the lignin model compounds catechol, resorcinol and hydroquinone. *Chemical Science* **2021**, *12* (9), 3161−3169. Kulik, T. V.; Lipkovska, N. O.; Barvinchenko, V. M.; Palyanytsya, B. B.; Kazakova, O. A.; Dudik, O. O.; Menyhárd, A.; László, K. Thermal transformation of bioactive caffeic acid on fumed silica seen by UV−Vis spectroscopy, thermogravimetric analysis, temperature programmed desorption mass spectrometry and quantum chemical methods. *J. Colloid Interface Sci.* **2016**, *470*, 132−141.

(35) Kulik, T. V.; Lipkovska, N. A.; Barvinchenko, V. N.; Palyanytsya, B. B.; Kazakova, O. A.; Dovbiy, O. A.; Pogorelyi, V. K. Interactions between bioactive ferulic acid and fumed silica by UV−vis spectroscopy, FT-IR, TPD MS investigation and quantum chemical methods. *J. Colloid Interface Sci.* **2009**, *339* (1), 60−68.

(36) Rimola, A.; Costa, D.; Sodupe, M.; Lambert, J.-F.; Ugliengo, P. Silica Surface Features and Their Role in the Adsorption of Biomolecules: Computational Modeling and Experiments. *Chem. Rev.* **2013**, *113* (6), 4216−4313.

(37) Cvetanović, R. J.; Amenomiya, Y. A Temperature Programmed Desorption Technique for Investigation of Practical Catalysts. *Catalysis Reviews* **1972**, *6* (1), 21−48.

(38) Hubbard, A. T. *The Handbook of Surface Imaging and Visualization*; CRC PressINC, 1995. Nicholl, S. I.; Talley, J. W. Development of thermal programmed desorption mass spectrometry methods for environmental applications. *Chemosphere* **2006**, *63* (1), 132−141.

(39) Redhead, P. A. Thermal desorption of gases. *Vacuum* **1962**, *12* (4), 203−211.

(40) Frisch, M. J.; Trucks, G. W.; Schlegel, H. B.; Scuseria, G. E.; Robb, M. A.; Cheeseman, J. R.; Scalmani, G.; Barone, V.; Petersson, G. A.; Nakatsuji, H.; Li, X.; Caricato, M.; Marenich, A.; Bloino, J.; Janesko, B. G.; Gomperts, R.; Mennucci, B.; Hratchian, H. P.; Ortiz, J. V.; Izmaylov, A. F.; Sonnenberg, J. L.; Williams-Young, D.; Ding, F.; Lipparini, F.; Goings, J.; Peng, B.; Petrone, A.; Henderson, T.; Ranasinghe, D.; Zakrzewski, V. G.; Gao, J.; Rega, N.; Zheng, G.; Liang, W.; Hada, M.; Ehara, M.; Toyota, K.; Fukuda, R.; Hasegawa, J.; Ishida, M.; Nakajima, T.; Honda, Y.; Kitao, O.; Nakai, H.; Vreven, T.; Throssell, K.; Montgomery, Jr., J. A.; Peralta, J. E.; Ogliaro, F.; Bearpark, M.; Heyd, J. J.; Brothers, E.; Kudin, K. N.; Staroverov, V. N.; Keith, T.; Kobayashi, R.; Normand, J.; Raghavachari, K.; Rendell, A.; Burant, J. C.; Iyengar, S. S.; Tomasi, J.; Cossi, M.; Millam, J. M.; Klene, M.; Adamo, C.; Cammi, R.; Ochterski, J. W.; Martin, R. L.; Morokuma, K.; Farkas, O.; Foresman, J. B.; Fox, D. J. *Gaussian09, Revision D.01*. http://www.gaussian.com/ (accessed October 23, 2023) , Gaussian, Inc.: Wallingford CT, 2013.

(41) Sauer, J. Molecular models in ab initio studies of solids and surfaces: from ionic crystals and semiconductors to catalysts. *Chem. Rev.* **1989**, *89* (1), 199−255. Zhidomirov, G. M.; Mikheikin, I. D. Cluster Approximation in Quantum-chemical Studies of Chemisorption and Surface Stnictures [in Russian]. *Progress in Science and Technology. Structure of Molecules and the Chemical Bond* 1984, *9*. All-Union Inst. of Scientific and Technical Information (VINITI), Akad. Nauk SSSR.

(42) Marshall, K.; Rochester, C. H. Infrared study of the adsorption of oleic and linolenic acids onto the surface of silica immersed in carbon tetrachloride. *J. Chem. Soc., Faraday Trans* **1975**, *71*, 1754−1761. Brei, V. V.; Brichka, A. V. *A Study of the Brönsted Site Acidity of Crystalline and Amorphous Aluminosilicates: 2. Thermal Decomposition of Grafted Acetyl Groups*. Adsorption Science & Technology 1996, *14* (6), 359−362. DOI: DOI: 10.1177/026361749601400603. Young, R. P. Infrared spectroscopic studies of adsorption and catalysis. Part 3. Carboxylic acids and their derivatives adsorbed on silica. *Can. J. Chem.* **1969**, *47* (12), 2237−2247. Basyuk, V. A. Infrared spectra of carboxylic compounds on silica surfaces at 1500−1800 $cm^{-1}$. *J. Appl. Spectrosc.* **1994**, *60* (1), 29−33. Martinez, R.; Huff, M. C.; Barteau, M. A. Synthesis of ketenes from carboxylic acids on functionalized silica monoliths at short contact times. *Applied Catalysis A: General* **2000**, *200* (1), 79−88.

(43) Azizova, L. R.; Kulik, T. V.; Palianytsia, B. B.; Lipkovska, N. A. Thermal and hydrolytic stability of grafted ester groups of carboxylic acids on the silica surface. *J. Therm. Anal. Calorim.* **2015**, *122* (2), 517−523.

(44) Zhuravlev, L. T. The surface chemistry of amorphous silica. Zhuravlev model. *Colloids Surf., A* **2000**, *173* (1), 1−38.

(45) Rimola, A.; Ugliengo, P. A quantum mechanical study of the reactivity of $(SiO)_2$-defective silica surfaces. *J. Chem. Phys.* **2008**, *128* (20), 204702. Rozanska, X.; Delbecq, F.; Sautet, P. Reconstruction and stability of $\beta$-cristobalite 001, 101, and 111 surfaces during dehydroxylation. *Phys. Chem. Chem. Phys.* **2010**, *12* (45), 14930−14940.

(46) Guo, J.; Han, A.-J.; Yu, H.; Dong, J.-p.; He, H.; Long, Y.-C. Base property of high silica MFI zeolites modified with various alkyl amines. *Microporous Mesoporous Mater.* **2006**, *94* (1), 166−172. Han, A.-J.; He, H.-Y.; Guo, J.; Yu, H.; Huang, Y.-F.; Long, Y.-C. Studies on structure and acid−base properties of high silica MFI-type zeolite modified with methylamine. *Microporous Mesoporous Mater.* **2005**, *79* (1), 177−184.

(47) Parfitt, G. D.; Rochester, C. H. *Adsorption from solution at the solid/liquid interface*; Academic Press, 1983.

(48) Gregg, S. J.; Sing, K. S. W. *Adsorption, surface area, and porosity*; Academic Press, 1982.

(49) Bellamy, L. J. *The infrared spectra of complex molecules: advances in infrared group frequencies. Vol. 2*; Chapman and Hall, 1980.

(50) Bromley, S. T.; Zwijnenburg, M. A.; Maschmeyer, T. Two-ring vibrational modes on silica surfaces investigated via fully coordinated nanoclusters. *Surf. Sci.* **2003**, *539* (1−3), L554−L559. Ceresoli, D.; Bernasconi, M.; Iarlori, S.; Parrinello, M.; Tosatti, E. Two-Membered Silicon Rings on the Dehydroxylated Surface of Silica. *Phys. Rev. Lett.* **2000**, *84* (17), 3887−3890. Lopez, N.; Vitiello, M.; Illas, F.; Pacchioni, G. Interaction of $H_2$ with strained rings at the silica surface from ab initio calculations. *J. Non-Cryst. Solids* **2000**, *271* (1−2), 56−63.

(51) Schnetzer, F. *The Interaction of Water and 2:1 Layer Silicates*; Karlsruher Instituts für Technologie 2017.

(52) Kamitsos, E. I.; Patsis, A. P.; Kordas, G. Infrared-reflectance spectra of heat-treated sol-gel-derived silica. *Phys. Rev. B* **1993**, *48* (17), 12499−12505. Wood, D. L.; Rabinovich, E. M. Study of Alkoxide Silica Gels by Infrared Spectroscopy. *Appl. Spectrosc.* **1989**, *43* (2), 263−267.

(53) Deacon, G. B.; Phillips, R. J. Relationships between the carbon-oxygen stretching frequencies of carboxylato complexes and the type of carboxylate coordination. *Coord. Chem. Rev.* **1980**, *33* (3), 227−250.

(54) Costa, T. M. H.; Gallas, M. R.; Benvenutti, E. V.; da Jornada, J. A. H. Infrared and thermogravimetric study of high pressure consolidation in alkoxide silica gel powders. *J. Non-Cryst. Solids* **1997**, *220* (2), 195−201.

(55) Abdallah, M. R.; Hasan, M. A.; Zaki, M. I. Theoretical Study of the Adsorption of 2-Propanol onto Silica Surfaces on the Basis of Ab Initio and Density Functional Calculations. *Adsorption Science & Technology* **2009**, *27* (3), 215−253.

(56) Foster, J. P.; Weinhold, F. Natural hybrid orbitals. *J. Am. Chem. Soc.* **1980**, *102* (24), 7211−7218.

(57) Becerra, A. J.; Martinez, R.; Huff, M. C.; Barteau, M. A. Catalytic synthesis of butylketene and hexylketene from hexanoic acid and octanoic acid on functionalized silica monoliths at short contact times. *Catal. Today* **2005**, *107−108*, 244−249. Maquestiau, A.; Flammang, R.; Pauwels, P. Mass and kinetic energy spectrometries of alkylketenes. *Organic Mass Spectrometry* **1983**, *18* (12), 547−552.

(58) Kulik, T. V.; Palyanitsa, B. B.; Azizova, L. R.; Tarnavskiy, S. S. Comparative mass-spectrometric study on the interaction of linear



https://doi.org/10.1021/jacs.3c06966
J. Am. Chem. Soc. XXXX, XXX, XXX−XXX

and branched homologs of valerianic and pivalinic acids with silica surface. *Surface* **2007**, *13*, 75−79, DOI: 10.15407/Surface.
(59) Lide, D. R. *CRC Handbook of Chemistry and Physics*, 90*th ed.*; Taylor & Francis, 2010.
(60) Leo, A.; Hansch, C.; Elkins, D. Partition coefficients and their uses. *Chem. Rev.* **1971**, *71* (6), 525−616.
(61) Sangster, J. Octanol-Water Partition Coefficients of Simple Organic Compounds. *J. Phys. Chem. Ref. Data* **1989**, *18* (3), 1111−1229.
(62) Armistead, C. G.; Tyler, A. J.; Hambleton, F. H.; Mitchell, S. A.; Hockey, J. A. Surface hydroxylation of silica. *J. Phys. Chem.* **1969**, *73* (11), 3947−3953.
(63) Technology, N. I. o. S. a. *NIST Mass Spectral Library*; National Institute of Standards and Technology:: Gaithersburg, MD, 2023.
(64) Dyker, G. Silica-Mediated Monohydrolysis of Dicarboxylic Esters. *Eur. J. Org. Chem.* **2021**, *2021* (48), 6773−6776.
(65) McLafferty, F. W. Mass Spectrometric Analysis. *Molecular Rearrangements. Analytical Chemistry* **1959**, *31* (1), 82−87.
(66) Kubátová, A.; Geetla, A.; Casey, J.; Linnen, M. J.; Seames, W. S.; Smoliakova, I. P.; Kozliak, E. I. Cleavage of Carboxylic Acid Moieties in Triacylglycerides During Non-Catalytic Pyrolysis. *J. Am. Oil Chem. Soc.* **2015**, *92* (5), 755−767. Kubátová, A.; Šťávová, J.; Seames, W. S.; Luo, Y.; Sadrameli, S. M.; Linnen, M. J.; Baglayeva, G. V.; Smoliakova, I. P.; Kozliak, E. I. Triacylglyceride Thermal Cracking: Pathways to Cyclic Hydrocarbons. *Energy Fuels* **2012**, *26* (1), 672−685. Kozliak, E.; Sulkes, M.; Alhroub, I.; Kubátová, A.; Andrianova, A.; Seames, W. Influence of early stages of triglyceride pyrolysis on the formation of PAHs as coke precursors. *Phys. Chem. Chem. Phys.* **2019**, *21* (36), 20189−20203. Dutta, S.; Madav, V.; Joshi, G.; Naik, N.; Kumar, S. Directional synthesis of aviation-, diesel-, and gasoline range hydrocarbon fuels by catalytic transformations of biomass components: An overview. *Fuel* **2023**, *347*, No. 128437.
(67) Gallorini, R.; Aquilia, S.; Bello, C.; Ciardelli, F.; Pinna, M.; Papini, A. M.; Rosi, L. Pyrolysis of spent rapeseed meal: A circular economy example for waste valorization. *Journal of Analytical and Applied Pyrolysis* **2023**, *174*, No. 106138. Sun, Y.; Li, C.; Zhang, S.; Dong, D.; Gholizadeh, M.; Wang, S.; Hu, X. Pyrolysis behaviors of rapeseed meal: products distribution and properties. *Biomass Conversion and Biorefinery* **2023**, *13* (8), 6575−6590. US Department of Agriculture, u. F. *Leading producing countries of rapeseed in 2022/2023 (in million metric tons)**. Statista, **2023**. https://www.statista.com/statistics/263930/worldwide-production-of-rapeseed-by-country/ (accessed 2023 September 19).
(68) Service, U. S. D. O. A. F. A. *Oilseeds: World Markets and Trade*. 2023. https://apps.fas.usda.gov/psdonline/circulars/oilseeds.pdf (accessed 2023 September 19).
(69) Bauer, B.; Kostik, V.; Gjorgjeska, B. Fatty acid composition of seed oil obtained fro different canola varieties. *Farmaceutski glasnik* **2015**, *71* (1), 1−7. Flakelar, C. L.; Adjonu, R.; Doran, G.; Howitt, J. A.; Luckett, D. J.; Prenzler, P. D. Phytosterol, Tocopherol and Carotenoid Retention during Commercial Processing of Brassica napus (Canola) Oil. *Processes* **2022**, *10* (3), 580. Tileuberdi, N.; Turgumbayeva, A.; Yeskaliyeva, B.; Sarsenova, L.; Issayeva, R. Extraction, Isolation of Bioactive Compounds and Therapeutic Potential of Rapeseed (Brassica napus L.). *Molecules* **2022**, *27* (24), 8824.
(70) Matthaus, B.; Özcan, M. M.; Juhaimi, F. A. Some rape/canola seed oils: fatty acid composition and tocopherols. *Zeitschrift für Naturforschung C* **2016**, *71* (3−4), 73−77. Akbari, F.; Khodadadi, S.; Asgary, S.; Shirzad, H.; Mirhoseini, M.; Shahinfard, N.; Rafieian-kopaei, M. A comparative study on hypoglycemic properties, lipid profile and bioactive components of hydro-alcoholic extracts of cooked and raw Brassica napus. *J. Nephropharmacol.* **2015**, *5* (2), 86−90.
(71) Kislyuk, M. U.; Rozanov, V. V. Temperature-Programmed Desorption and Temperature-Programmed Reaction as Methods for Studying the Kinetics and Mechanism of Heterogeneous Catalytic Processes. *Kinetics and catalysis* **1995**, *26* (30), 80. Carter, G. Thermal resolution of desorption energy spectra. *Vacuum* **1962**, *12* (5), 245−254. Woodruff, D. P.; Delchar, T. A. *Modern Techniques of Surface Science*; Cambridge University Press, 1986.
(72) Lebedev, A. T. Introduction to Mass Spectra Interpretation: Organic Chemistry. In *Mass Spectrometry*, 2008; pp 119−178. McLafferty, F. W.; Turecek, F. *Interpretation Of Mass Spectra*; University Science Books, 1993.


https://doi.org/10.1021/jacs.3c06966
J. Am. Chem. Soc. XXXX, XXX, XXX−XXX